UMEÅ UNIVERSITY

MASTER THESIS

Neural network based fault detection on painted surface

Author:
Midhumol Augustian

A thesis submitted in partial fulfillment of the requirements for the degree of Masters in Robotics and Control Engineering

Department of Applied Physics and Electronics
Umeå University

2017

Declaration of Authorship

I, Midhumol Augustian, declare that this thesis titled, "Neural network based fault detection on painted surface " and the work presented in it are my own. I confirm that:

- This work was done wholly while in candidature for a Masters degree in Robotics and control Engineering at Umeå University.
- Where I have consulted the published work of others, this is always clearly attributed.
- Where I have quoted from the work of others, the source is always given. With the exception of such quotations, this thesis is entirely my own work.
- I have acknowledged all main sources of help.
- Where the thesis is based on work done by myself jointly with others, I have made clear exactly what was done by others and what I have contributed myself.

Signed:

Date:

Abstract

Machine vision systems combined with classification algorithms are being increasingly used for different applications in the age of automation. One such application would be the quality control of the painted automobile parts. The fundamental elements of the machine vision system include camera, illumination, image acquisition software and computer vision algorithms. Traditional way of thinking puts too much importance on camera systems and ignores other elements while designing a machine vision system. In this thesis work, it is shown that selecting an appropriate illumination for illuminating the surface being examined is equally important in case of machine vision system for examining specular surface. Knowledge about the nature of the surface, type and properties of the defect to be detected and classified are important factors while choosing the illumination system for the machine vision system. The main illumination system tested were bright field, dark field and structured illumination and out of the three, dark field and structured illumination gave best results.

This thesis work proposes a dark field illumination based machine vision system for fault detection on specular painted surface. A single layer Artificial Neural Network model is employed for the classification of defects in intensity images of painted surface acquired with this machine vision system. The results of this research work proved that the quality of the images and size of data set used for training the Neural Network model play a vital role in the performance of the classifier algorithm.

Keywords: Specular surface, Machine vision system, Automatic inspection, Dark field illumination, Structured illumination, Artificial Neural Network classifier.

Acknowledgements

This thesis provided me with an exciting opportunity to learn and to acquire a great deal of knowledge. I am extremely thankful to Volvo Group Trucks Operations, Umeå and Mr. Kent Sundberg (Manager, Engineering Support & IT at Volvo GTO, Umeå) for believing in my abilities and presenting me with this wonderful opportunity.

I would like to extend my sincere gratitude to my supervisors Assoc. Prof. Shafiq Ur Réhman, Dr. Muhammad Sikandar Lal Khan and Mr. Carl Marton for their great guidance and mentorship.

I gratefully acknowledge my examiner Assoc. Prof. John Berge for his excellent support during the thesis.

I take this opportunity to thank Ms. Yongcui Mi for being an inspiring team mate. Her hard work and commitment always motivated me to strive to achieve the goals of this thesis.

I would like to thank the employees at the mechanical workshop at Volvo plant, Umeå for their excellent help with the mechanical setup of the machine vision system.

Midhumol Augustian
Umeå, Sweden, 2017

Contents

List of Figures

List of Abbreviations

ANN	**A**rtificial **N**eural **N**etwork
HOG	**H**istogram of **O**riented **G**radients
TPR	**T**rue **P**ositive **R**ate
FPR	**F**alse **P**ositive **R**ate
TP	**T**rue **P**ositives
FP	**F**alse **P**ositives
TN	**T**rue **N**egatives
FN	**F**alse **N**egatives
ROC	**R**eceiver **O**perating **C**urve
FOV	**F**ield **O**f **V**iew
SVM	**S**upport **V**ector **M**achine
LBP	**L**ocal **B**inary **P**attern
RGB	**R**ed **G**reen **B**lue
IR	**I**nfra **R**ed

Chapter 1

Introduction

Nowadays, machine vision is being increasingly used for various quality control processes. The main advantage with machine vision system is that it makes visual information understandable and illustrative. Machine vision systems' major components consist of image acquisition devices, illuminations, computing devices, and sophisticated algorithms. In the era of industrial automation, machine vision can play a vital role in applications like automatic inspection and quality control processes. One such application could be the fault detection on painted automobile surface.

Final surface appearance is a key factor for customer satisfaction in automobile industry. Even though each product is treated with a continues painting process under controlled conditions to ensure the high quality, flaws on the painted surface are inevitable due to the presence of dust, fibers etc. Today final painted surface inspections are manual visual inspection by quality inspectors which are susceptible to inconsistency due to unavoidable human errors. The quality inspectors examine the painted surface in the final stage under quite uncomfortable conditions: they use their eyes and hands as their tools within a limited time for the inspection of each cab. This consequently leads to less reliable and inconsistent defect detection. Moreover, there are some defects that workers are unable to discover, due to their micrometer size, or their less-accessible location on the product. Some defects are visible only in some viewing angles making the inspection process more difficult for the worker. Therefore, automobile manufacturers have a strong desire to replace this manual inspection with a cost effective and efficient machine vision based inspection system.

Painted truck bodies are very difficult to inspect because of their specular nature, different shape, surface details, and wide variety of color combinations. The main objective of this thesis is to select, design and construct a prototype of machine vision inspection system for defect detection on specular painted truck bodies. The basic requirement of the system is to detect defects of micrometer size on test slabs collected from painting work shop. Then with the help of different computer vision techniques these small sized defects are detected. Machine learning approaches like Artificial Neural Network is employed for the classification of defect types. This thesis has a great significance since the thesis will provide knowledge for the automation of

a manual inspection process by applying artificial vision techniques for the detection of small defects on specular surfaces.

1.1 Aim of the thesis

The over all aim of the thesis is to propose a vision based defect detection solution for the paint fault inspection unit to make it more effective. The thesis goals are listed below.

1. Study and investigate on feasible machine vision system for fault detection on specular painted surface.
2. Evaluate the performance of sensors, optics and illumination on test slab surfaces and propose a machine vision system for fault detection on specular painted surfaces.
3. Employ machine learning algorithms for the classification of defects on intensity images of test slabs captured with proposed machine vision system.

1.2 Requirement specifications

The requirements to be satisfied by the machine vision system are :

- The machine vision system should be able to inspect on painted automobile surface which is specular surface.
- The machine vision system should also be able to detect defects that have a micrometer range size.
- The fault detection system should be able to inspect on different color combination of painted surface irrespective of the color.

1.3 Delimitations

The limitations of this thesis work are :

- This thesis work is mainly focused on intensity images rather than on deflectometry images.
- For the selection of machine vision system, testing was carried out on painted slabs (20x10 cm) collected from painting workshop. This slabs are flat and do not contain any surface details.
- Even though there are different types of defects present on painted surface truck surface, it is difficult to gather slabs with all these defects.

There for, the thesis work only considered two major defect types dirt and crater.

1.4 Thesis outline

This thesis is structured as follows. Chapter 2 gives an account on the specular nature of the painted surface and defect types. This chapter also discuss various machine vision techniques and computer vision techniques for fault inspection on specular surface. Chapter 3 outlines the methodology followed in this thesis. This chapter includes description of machine vision components tested in this work, theory of various computer vision techniques employed in this thesis and a description of Artificial Neural Network classifier. In Chapter 4, various results of this thesis work are presented. The results section consists of three parts. In the first part of this chapter a proposal of machine vision system for fault detection on painted surface is presented. In the second section, results of pre-processing and various computer vision methods are presented. The final section of this chapter presents the results of classification of defects with Artificial Neural Network model. Chapter 5 gives a summary and future work suggestions of this work.

Chapter 2

Theory and background

The nature of the surface to be inspected is a very important factor while choosing a system to inspect the surface. The type of defects to be detected is another important factor with regard to selecting fault detection system and computer vision algorithms. In this chapter an account on the nature of the painted surface and defect types are given in sections 2.1 and 2.2. Section 2.3 talks about various machine vision system for fault inspection on specular surface. This section discuss in detail various components of machine vision system as well. Next section 2.4 deals with different computer vision techniques to detect defects on specular surfaces. Works of various researchers in specular surface fault detection is also presented in this section. In the final section of this chapter a study on existing paint fault inspection system is presented.

2.1 Specular nature of painted surface

Machine vision techniques are highly dependent on nature of the surface to be inspected and characteristics of defects. Because of this reason it is important to investigate the nature of the painted surface. The painted truck body surfaces are highly specular reflective in nature. Shiqing et al. [1] in their article categorized reflection on a surface into specular (mirror like) and diffused reflection. In diffused reflection incident light ray is scattered by the surface and hence luminance of the surface is same in all viewing angle. Lambertian reflectance model describes this kind of diffusely reflecting surfaces [2].

Specular reflection is a surface phenomenon in which angle of incidence of light rays equals the angle of reflection of reflected light rays [1]. Nayar reflectance model is widely used to explain the surface reflection. Nayar model consists of three primary reflectance components: specular lobe, specular spike, and diffuse lobe [2] as shown in figure 2.2. With the increase in surface roughness specular spike will start to diminish and specular lobe becomes more dominant. Further increase in roughness causes the dominance of diffuse lobe.

Pradeep et al. [3] in their work presented that, for highly specular surfaces specular spike is much greater than the specular lobe and diffuse component

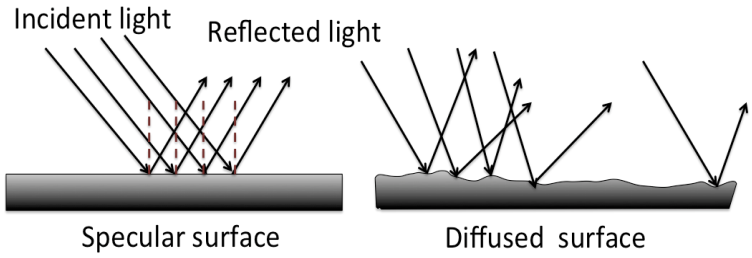

FIGURE 2.1: Illustration of reflection on specular and diffuse surfaces.

is negligible. This concentration of light energy along specular lobe causes strong highlights in the images. Also Chang et al. [4] reported that highly specular reflective surfaces with very weak diffuse reflection makes the surface inspection a challenging task, since this kind of surfaces are too sensitive to illumination direction to form a acceptable surface information.

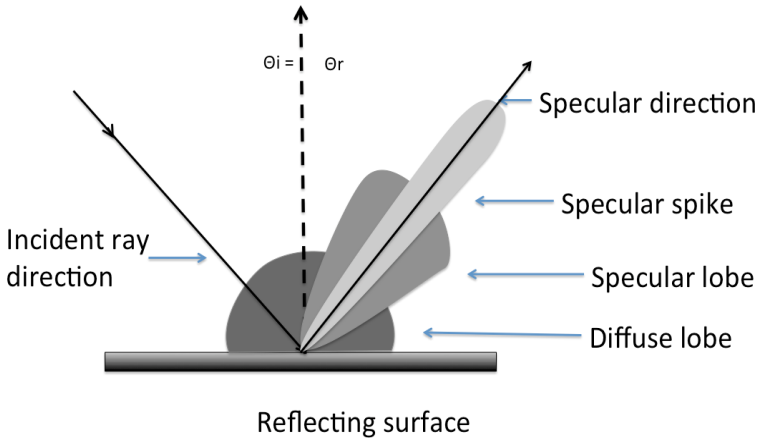

FIGURE 2.2: Nayar reflection model.

2.2 Painted surface defects

Automotive paint is applied as various coats one after another. These painting coats include e-coat, primer coat, base coat and clear coat [5]. Base coat determines the color and visual appearance of vehicle surface. The main color type available are solid, metallic and pearl. Presence of aluminium chips gives a sparkling effect for metallic surface. Since 87.47% of painted truck surface are solid surface, the images were mainly collected from the solid surface for the fault detection.

Automotive painting is a continuous process and surface flaws can occur during this process. This paint defects can badly affect the final surface appearance of the automobile. Some defects can be measurable and some of them are not.

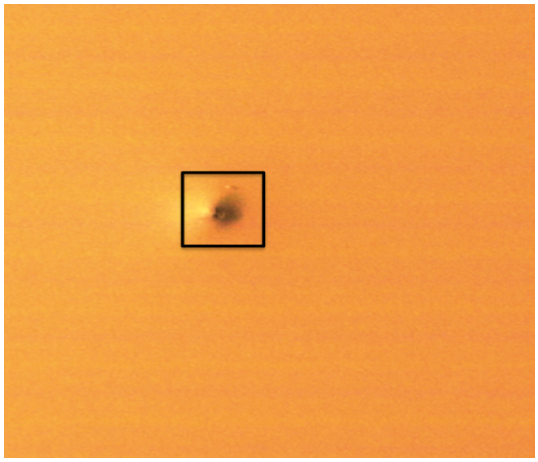

(A) Dirt on solid surface

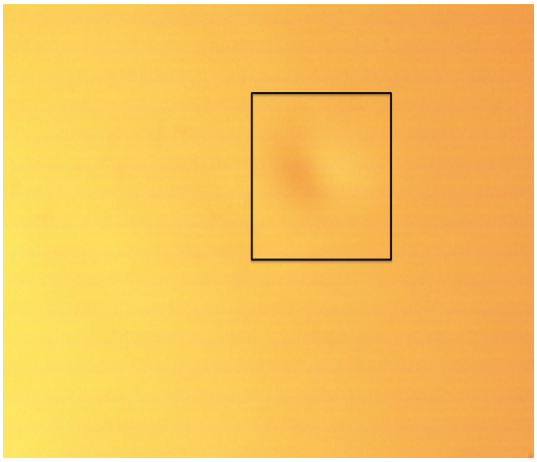

(B) Crater on solid surface

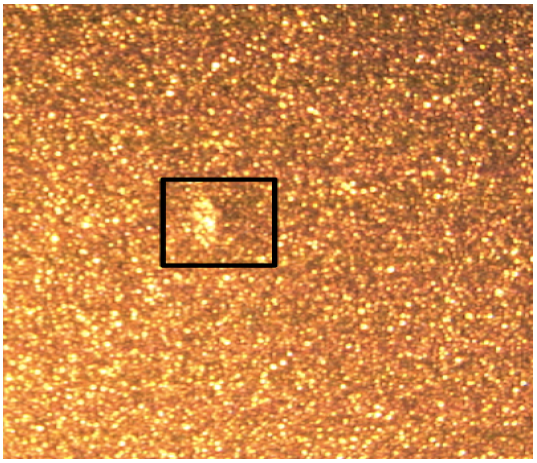

(C) Dirt on metallic surface

FIGURE 2.3: Microscopic view of defects on automotive painted surface.

Major measurable defects found on painted truck surfaces are explained below.

- Dirt

  Dirt is caused by the presence of foreign particle in the paint. This foreign particle can be dust or fibers.

- Crater

  Crater is appeared as a circular volcano with raised edge. The reason for crater is the difference in surface tension caused by contaminants in the paint.

- Surface scratch

  Main reason for surface scratch is mechanical damage on the top coat.

- Drips/ Runs

  Drip is appeared as uneven coating caused by accumulation of paint.

There are non-measurable paint defects like color difference, over spray, dry spray, polishing marks etc. are also present on the painted surface.

It is clear from the figure 2.3 that crater appears as a curvature defect. This kind of defects are visible only in some angles which make it difficult to capture by a machine vision camera. Also speckles in metallic surface may be confused with defect by the fault detection algorithms. Hence the selection of machine vision system and computer vision algorithms are critical to ensure the performance of painted surface inspection system. The following sections in this chapter gives an overview of various components of a machine vision system and different computer vision techniques for specular surface inspection.

2.3 Machine vision system

For a painted surface inspection the machine vision system requires a quality image to detect the defects. In a generic view we can say that a machine vision system should be able to produce high contrast between features of interest (defects) and the intact surface. Machine vision system consists of camera, lenses, illumination, software for image acquisition and sophisticated computer vision algorithm for processing the images. Major machine vision techniques for specular surface inspection are *intensity imaging* [6] and *phase shifting* [7]. This distinction is based on the illumination used in machine vision system. The following subsections give an account on the key components of machine vision system.

2.3.1 Camera

Ajay [8] in his work presented two scanning techniques to scan the surface : one is line scanning and other one is area scanning. Line scanning cameras utilizes linear array of photo-sensors and its images are one dimensional. In order to cover a large area either line scan camera or object is required to move. The main advantage of line scan camera is that it can provide high resolution images. The disadvantage of this technique is that in order to create a complete image of a surface it requires an external hardware to join all these lines. Since the cost of line scan is high, currently an array of area scan cameras are widely used in machine vision applications to cover a large area. Area scan camera can provide two dimensional image in a single exposure.

The working priciple of camera is that the incoming light from object is converted to electrical signal by the photo sensor. This sensors can either be CCD (charge coupled device) or CMOS (complimentary metal oxide semiconductor). The produced electricity is proportional to intensity of the incoming light [9]. CMOS sensors can have more on-chip functionality than its counterpart CCD sensor[10]. In this work the selected cameras for testing are

equipped with CMOS sensors. The fundamental parameters of camera need to be considered while selecting a machine vision camera are:

- Resolution

  Resolution is the smallest distinguishable feature a camera can capture without being blurred. It is measured in pixels. Camera with smaller pixel size has higher resolution image and can capture more details of the object under inspection.

- Field of view

  The area of the object under inspection that camera can capture.

- Working distance

  The distance between front part of lens to the object under inspection.

- Depth of Field

  It is the zone between nearest and farthest points in a scene that can appear sharp in an image. Depth field is also known as focus range.

- F number

  It is the ratio of focal length to the aperture of entrance pupil of lens. F number is a dimensionless quantity. Smaller F number means larger aperture diameter of pupil of lens.

Suitable lenses are also required to focus the camera on to the desired field of view of the surface. Lenses help to increase the contrast between background and features of interest. Various conventional lenses and telecentric lenses are availale in the market for machine vision applications. The advantage of telecentric lens over conventional lens is that it is able to produce an image with same magnification for all objects in a specified range. Because telecentric lens receives only light rays that are parallel to the optical axis. This advantage of avoiding perspective distortion with telecentric lenses are well suitable for metrology applications [11]. However telecentric lens has this property only over a range called telecentric depth. Beyond telecentric depth images will distort. For this reason telecentric lenses with long range are expensive than conventional lenses.

2.3.2 Illumination

The role of Illumination in machine vision system is to increase the visiblity of the features of interest. The quality of image is highly dependent on the illumination employed in the machine vision system [12]. Hence selecting a suitable illumination is crucial to ensure an effective fault detection on specular surface. Franz et al. [6] categorized illuminations used for surface inspection systems as *front lighting*, *back lighting* and *structured lighting* as illustrated in figure 2.4. For intensity imaging of reflective surfaces front lighting is relevant. Different types of front lighting techniques are availabe in the market.

They are comprised of diffused (full bright field), coaxial light (full bright field), directional bright field (partial bright field) and directional dark field illumination [13] .

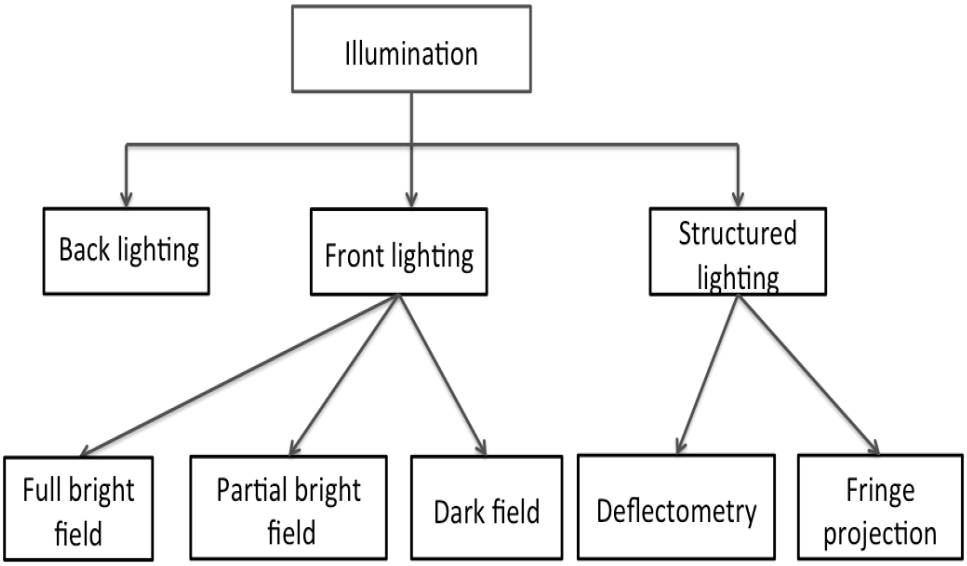

FIGURE 2.4: Block diagram representation of machine vision Illumination.

Diffuse lighting can provide uniform illumination and can eliminate shadows. But it will not be suitable for automobile industry, because of its sensitivy to uneven surface geometry [7]. Also it requires close proximity to the surface to be inspected for effective inspection. In directional bright field illumination the angle of incident light to the surface normal is small and this causes most of the light to fall on the camera sensor. Hence the surface will appear brighter and defects will appear darker in the captured image. With dark field illumination the angle of incident light to the surface is smaller and this subsequently leads to reflection of light away from the non-defective surface. The presence of defects cause the light to reflect towards the camera. Hence the image will be predominantly dark for non-defective area and brighter for defects with dark field illumination.

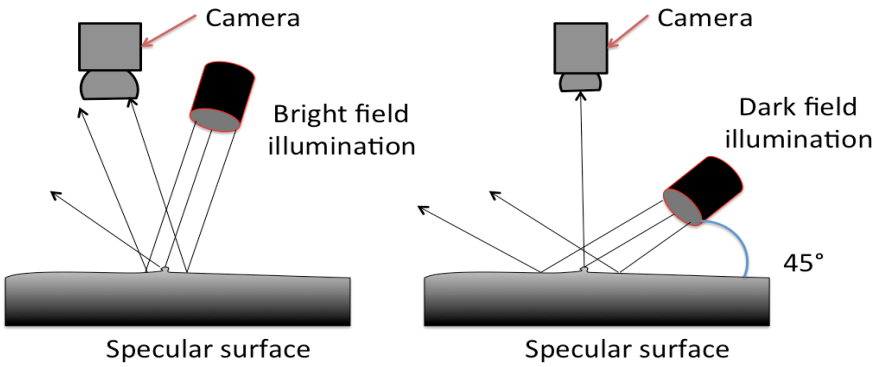

FIGURE 2.5: Principle of bright field and dark field illumination.

Abouelela et al. [14] proposed an automatic defect inspection system for textile fabric which employs infrared dark field lighting as illumination. They suggested that dark-field can be helpful in magnifying minute defects. In 1990 Piironen et al. [15] developed a automated visual inspection system for specular rolled metal surfaces. In their system a condensing bright field illuminators and CCD line scan camera were used as image acquisition system. Partial bright field illumination and dark field illumination setups were compared for the inspection of highly reflective rings by Ramamoorthy et al. [16]. In their work, dark field illumination setup images gave more accurate defect detection results than partial bright field illumination images.

The phase shifting methods like fringe projection and deflectometry employs a structured light pattern [7]. These patterns are projected onto the surface and then the displacement or distortion of pattern caused by slope variations of the surface is measured. Structured illumination is often used to obtain height map of the surface and especially for 3D inspection tasks [17]. Kammel et al. [18] gave a clear distinction between fringe projection method and deflectometry. In fringe projection, camera is focused on to the surface where the pattern is projected. Where as in deflectometry camera observes the reflection of the pattern displayed on the screen by the surface. Here the inspected surface is also a part of the optical system. Perard et al. [19] pointed out that unlike fringe projection method deflectometry is sensitive to small variations of the surface which is essential for measuring curvature defects like crater on the painted surface.

2.4 Computer vision techniques for fault detection on painted surfaces

The next step in machine vision system is to apply defect detection algorithms on captured images of the painted surface. According to Xie [20], major defect detection algorithms for intensity images can be classified into four categories:

1. Statistical approaches
2. Structural approaches
3. Filter based approaches
4. Model based approaches.

2.4.1 Statistical approaches

Statistical approaches measure the spatial distribution of pixel values. This method includes histogram approaches, local binary pattern (LBP) and histogram oriented gradients (HOG). Weimer et al. [21] in their work used statistical features like mean, standard deviation, central moments and Hu moments from image patches for the defect classification. Hu moments are rotational, translational and scale invariant [22]. Tajeripour et al. [23] performed defect detection on fabrics using LBP. In order to calculate LBP, image is divided into cells and the center pixel of the cell is compared with its circular neighborhood. Then the LBP histogram is computed over the cells. This LBP histograms are normalized and then concatenated to get a feature vector. HOG features counts the occurrences of gradient orientations over a local cell in an image. This features were utilized by Dalal et al. in their work for human detection [24] . Since intensity images have an eminent gradient orientation between defect and background, HOG features can also be a solution for defect detection.

2.4.2 Structural approaches

Structural approaches mainly consist of morphological operations. Basic morphological operations used for both binary and gray scale images are erosion, dilation, opening, and closing etc. Karimi et al.[25] suggested that an appropriate selection of structuring element greatly affects the performance of the morphological operations. Ling et al. [26] proposed a combination of Gabor wavelet network and morphological operators to detect defects in fabric texture. In this method, a pre-trained Gabor wavelet network was firstly used to design the structuring element of morphological methods. Then the input image successively passes through morphological operations and thresholding stages to identify the defects. Elbehiery et al. [27] successfully implemented defect detection on ceramic tiles by applying morphological operations.

2.4.3 Filter based approaches

Filter based approaches include Gabor filter, Wavelet transform and edge detection filters like Sobel, Canny, Laplacian, Robert and Deriche [20] for gray scale images. A Gabor function is a two-dimensional Gaussian modulated

sinusoidal plane wave with frequency and orientation. In 1991, Jain et al. performed an unsupervised learning of texture classification with Gabor filters [28]. Gabor filter can be seen as a preprocessing stage in defect detection. With Gabor filter it is possible to create a distinction between defects and background. Then a simple thresholding is required to extract the defect region [25].

Wavelet transforms with mother wavelets like Haar, Mexican Hat, Morlet etc are used to find the edges in the 2D images. Kamlesh et al. explained that 2D wavelet transform filter bank decompose a 2D image into approximation coefficients, and detail coefficients in three orientations (vertical, horizontal, and diagonal) [29]. The approximation coefficient contain low frequency component of the image and detail coefficient contains the high frequency component of the image. This provides us with different edges in the images and also can be used to denoise the image. Based on a 2-D Translation Invariant RI-Spline Wavelet Transform, Ren et al. [30] developed a novel automated defects detection system for metallic surfaces.

2.4.4 Model based approaches

Model based approaches can provide defect classification. The advantage of defect classification is that it helps in the diagnosis of similar defect types. The knowledge of defect type is very useful to repair the painted surface. Two major model based approaches suggested by Kamil et al. [31] are Artificial Neural Network (ANN) and Support Vector Machine (SVM). In their experiments Neural network provided more accurate results than SVM, but they pointed out that neural network is computationally more expensive than SVM.

Weimer et al. [21] successfully implemented a statistical feature based on two layer neural network for the detection of defects on textured surfaces. They used labeled features of with and without defects to train a model via back propagation learning. Later this trained model is tested with unlabeled features which is realized in sliding window fashion. Ramakrishnan et al. [32] performed a multilayer Gabor feature based neural network for texture classification. Kumar [33] used Principal Component Analysis (PCA) for feature extraction and trained a feed forward neural network based on these features.

2.5 Related work on paint fault inspection systems

Automatical Body Inspection System (ABIS) system is a unpainted car body inspection system to automatically detect defects like dents and ripples on car bodies during the production [34]. The main components of this system for online detection of defects are: twenty to twenty five range sensors and

robots. The sensor array scan the whole surface of the body to detect the defects and robots mark these detected defects areas. ABIS system is able to perform identification of the car type that enters the sensor portal, 3D data acquisition, detection, analysis, and classification of defects. But this system is restricted to detect defects on diffusively reflective surface like sheet metals.

D SIGHT is a real-time surface inspection system patented by Diffracto Ltd in Canada [35] to check defects on highly reflective surfaces (roughness less than 0.05 μm). The main components of this system consist of a camera, illumination, and a retro reflective screen. This system is capable of detecting minor out-of-plane surface defects on large highly specular surfaces. The efficiency of this system reduces with increasing roughness of the painted surface. The roughness of the surface must be less than 0.13 μm in order to make sure adequate performance of this system. Since the contrast of the defect is highly influenced by the ambient light, this system requires shielding while inspecting the surface.

The German sensor manufacturer Micro-Epsilon introduced reflectCONTROL for the inspection of painted car body surface [36]. The principle of inspection is based on deflectometry technique and this system is able to 3D reconstruct defects. To accomplish the surface inspection of a car, reflectCONTROL utilizes four robots working in parallel, each one of them equipped with a large monitor and four cameras. This inspection system takes less than one second for the inspection of a car. But its performance is affected by orange peel of the painted surface and ambient light in the inspection area.

Since all above mentioned online inspection systems are very expensive and are purely based on computer vision techniques, this thesis work investigates and propose much cheaper painted surface quality inspection system solution based on data driven approach.

Chapter 3

Methodology

This chapter discusses the methodology followed in this thesis. In section 3.1, a description of machine vision components tested in this work is presented. Theory of various computer vision techniques employed in this thesis is discussed in section 3.2. In section 3.3, a description of artificial neural network classifier and its feature set are presented.

3.1 Machine vision setup components

The sensors, optics, and Illuminations which were tested during the thesis work are listed below.

1. Sensors
    - **Genie Nano M2450 monochrome camera**: Genie Nano M2450 is a 5.1 MP monochrome camera with an image resolution of 2448 $\times$ 2048. It uses gigabit Ethernet as interface and data transfer is over Ethernet cable. Each pixel has a size of 3.45 μm which is smaller than the defect size. The image acquisition software supported by Gene camera is Common vision blox licensed by Stemmer imaging [37].
    - **Basler ace 2.3 MP monochrome camera**: Basler ace is a monochrome camera with a CMOS sensor. It has an image resolution of 1920 x 1200 and each pixel has a size of 5.86 μm. The data transfer is over USB 3.0 and image acquisition software is Matrox Design Assistant which is licensed by Matrox imaging [38].
2. Optics
    - **Telecentric lens**: TC 23036 telecentric lens has a working distance of 10.25 cm and a depth of field of 11 mm. Object should be kept in depth field range to ensure a sharp image of the object. The object field of view provided by TC23036 lens is equal to 6.1 cm. The distortion of the real image is less than 0.04 % [39].
    - **Kowa lens (Conventional lens)**: Kowa LM16 is a C mount lens with a manual focus control. The focal length of this lens is equal

to 16 mm and minimum focus range is 0.1 m. Kowa lens has F number between F1.8 and F16 [40].

3. Illuminations

   - **Dome light**: MB-DL406-RGB24ILD dome light is a diffused illumination suitable for curved specular surfaces. This illumination is available in RGB LED color. The power supply required for RGB dome light is 24 volt dc supply. The area covered by dome light is 17.78 cm diameter [41].
   - **Coaxial light**: PHLOX RGB LED on axis light can cover an area of 10cm x 10cm. The half mirror in the coaxial light reflects light from the side to the target. The specular reflection from the target is allowed to pass through the half mirror to the camera where as diffused reflection is blocked. This creates a contrast between defect and flawless surface [42].
   - **Ring light**: Three different dark field ring lights were tested on the slabs. They are: RGB color (HPR2-100FC), white color (HPR2-100SW) and Infrared (LDR2-90IR2-850) ring lights. RGB color and white color ring lights have an inner diameter of 66 mm. IR ring light has an inner diameter of 50 mm and has a peak wavelength of 850 nm [43].
   - **Bar light**: A White bar light (LDL2-266X30SW) and a 4 x Bar Light produced from LDL2-80X16SW were tested during the experiments. 4 x Bar light has got a diffusive cover over the light to produce diffusive light effect [44].
   - **Smart Color Box**: Smart color box helps to select a best suitable light color for the application by testing different light colors on test surface. It has six LED lights with white, red, blue, green, UV and IR variants. Each one can be selected by pushing a button behind the color box [45].

4. Software

   - **MATLAB**: All the pre-processing and defect detection algorithms were implemented in MATLAB. In built MATLAB functions for filters, morphological operations, wavelet transform, super pixel segmentation and HOG feature were utilized for the thesis work.
   - Image acquisition software Common vision blox
   - Image acquisition software Matrox Design Assistant

A test rig to mount the setup was made with aluflux aluminium profile and testing of setup was performed on test slabs of size of 20cm x 10cm collected from the paint workshop. Different combinations of sensors, optics and illuminations were tested on the test slabs. By visual inspection of the acquired images, a quick selection of lenses and illuminations were carried out. The

selected combinations of illumination and optics were evaluated by applying simple computer vision algorithms like morphological operations and various filters on acquired images.

Based on experiments, prototypes of two possible solutions of machine vision system for fault detection on painted truck body surface were set up in the lab environment. One possible solution, ring light setup is based on dark field illumination and the other solution deflectometry is based on structured illumination. The project was carried out in a group of two people. During the thesis it is decided that one team member will investigate dark field illumination setup and other team member investigate deflectometry setup. This work investigates dark field illumination setup with machine learning algorithms for defect detection.

Machine learning algorithms like artificial neural network was employed for the classification of defect types. Machine learning algorithm requires big data set for the learning. The data which is going to be used for classification are intensity images collected from the prototype of ring light setup. The classification will be based on dirt, scratch, and no defect area.

Various computer vision techniques and artificial neural network classifier employed in this work for defect detection and classification are discussed in detail in section 3.2 and 3.3 respectively.

3.2 Computer vision methods for image enhancement

The theoretical principles behind various computer vision methods employed during the thesis work for image enhancement are discussed in the following subsections. These computer vision techniques includes Gabor filter, wavelet transform and super pixel segmentation.

3.2.1 Gabor filter

A Gabor filter is generated by the modulation of a sinusoidal signal with a Gaussian function. Gabor filter response is similar to the response of visual cortex region of human brain[46]. The equation of gabor filter described by Daugman [47] is :

$$\begin{aligned} g_{\lambda,\theta,\phi,\sigma,\gamma}(x,y) &= exp\left(-\frac{x'^2+\gamma^2y'^2}{2\sigma^2}\right)cos\left(2\pi\frac{x'}{\lambda}+\varphi\right), \\ x' &= xcos\theta + ysin\theta, \\ y' &= -xsin\theta + ycos\theta, \end{aligned} \tag{3.1}$$

where λ is the wavelength and ψ is the phase offset of the cosine function in Gabor filter equation. σ represents standard deviation of the Gaussian function in Gabor filter equation and γ is the aspect ratio of the Gaussian function. θ represents orientation of the Gabor filter. The Gabor filter response of a 2-D image can be obtained by convolution of image with a Gabor filter bank.

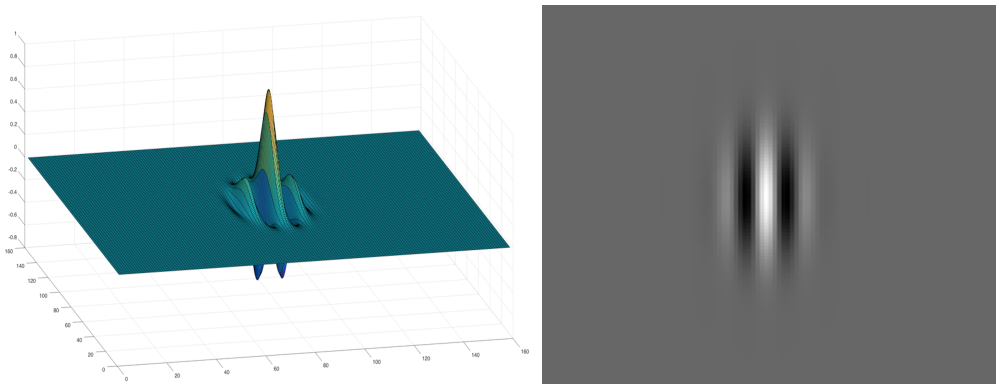

(A) 3D plot of Gabor filter (B) 2D plot of Gabor filter

FIGURE 3.1: Gabor filter with wavelength (λ) =10 and orientation (θ)=0.

A Gabor filter bank is generated by the combination of different wavelengths and orientations. Gabor filter with a wavelength of 10 pixels/cycles and orientation equal to $0°$ is demonstrated in figure 3.1. In order to obtain better results with Gabor filters, suitable wavelength and orientation should be chosen according to the application. Gabor filters are commonly applied for the analysis of image textures.

3.2.2 Wavelet transform

Wavelet transform can plot a signal in both frequency and time domain. A pyramidal algorithm proposed by Mallat utilizes a low pass and high pass filter banks for the decomposition of a 2D image [48] as demonstrated in figure 3.2.

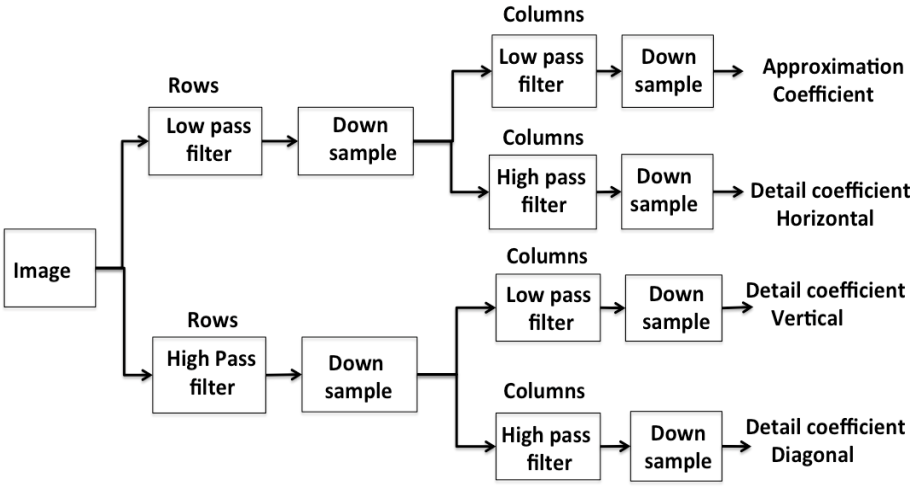

FIGURE 3.2: 2D wavelet decomposition.

In his approach, a two dimensional image is treated as a one dimensional wavelet transform in x and y direction. Wavelet filter bank decomposes a image in to approximation coefficient and detail coefficients in three orientations (horizontal, vertical and diagonal). The simplest wavelet type Haar wavelet can be represented as given in formula 3.2.

$$\psi = \begin{cases} 1 & 0 \leq t < \frac{1}{2}, \\ -1 & \frac{1}{2} \leq t < 1, \\ 0 & \text{Otherwise.} \end{cases} \tag{3.2}$$

3.2.3 Super pixel segmentation

Super pixel is a collection of neighboring pixels with similar intensity values or texture representation. With super pixel segmentation it is possible to divide an image into non-overlapping super pixels. Super pixel reduces the complexity of segmentation with single pixel. MATLAB *superpixels* function utilizes Simple Linear Iterative Clustering (SLIC) algorithm proposed by Achanta et al. [49] to perform super pixel segmentation.

This approach is performed in five dimensional *labxy* space by clustering pixels that are closer and having similar color [50]. $[l, a, b]^T$ represents color vector of pixel in CIELAB color space and $[x, y]^T$ represents coordinate of pixel in two dimensional space. Acronym *l* in *lab* corresponds to lightness, *a* and *b* correspond to two color channels (green-red and blue-yellow). The input to the super pixel function is the number of super pixels (K). For an N pixel image the possible size of super pixel is $\frac{N}{k}$ and the grid interval S is equal to $\sqrt{N/K}$. K number of initial cluster centers are assigned to the grid intervals as $C_k = [l_k, a_k, b_k, x_k, y_k]^T$. Then this clusters are moved to the lowest gradient position in its neighborhood to avoid clustering of super pixel near an

edge. For each pixel in the 2S×2S region around the center C_k, the distance between center and pixel (D_s) is calculated based on the formula 3.3.

$$\begin{aligned} d_{lab} &= \sqrt{(l_k - l_i)^2 + (a_k - a_i)^2 + (b_k - b_i)^2} \\ d_{xy} &= \sqrt{(x_k - x_i)^2 + (y_k - y_i)^2} \\ D_s &= d_{lab} + \frac{m}{S} d_{xy} \end{aligned} \tag{3.3}$$

With larger m value, more weight is given to spatial proximity and with smaller m value more weight is given to color similarity. After each pixel is associated with a cluster, the cluster center is updated with the average of the $[l, a, b, x, y]^T$ vector. This process is repeated until the error between new cluster center and previous cluster center is less than a previously assigned threshold value.

3.3 Artificial neural network

An artificial neural network is inspired by human brain functionality consists of input nodes (or neurons), hidden layers and output nodes [51]. These layers are connected by links and the strength of each link is known as its weight. Artificial neural network model that was implemented has input and output layers as shown in figure 3.3 and does not have any hidden layers. The number of input layers depend on the size of features vector created for the ANN model training. The output layer have three nodes. Each node corresponds to no defect, dirt and scratch respectively.

Training of artificial neural network comprises of two main steps. The first one is feed forward propagation and the other one is backward propagation. In feed forward step the weights of the neural network links are randomly initialized and then the value for each output node is computed. Since the data set for training is labeled the desired output for each node is known. The weights of each link are updated in back propagation step in order to reduce the error margin in the output node signal. The weight matrix corresponds to three layer output nodes and input layer size (HOG feature size) of 1× 576 is given in equation 3.4. The size of weight matrix is 3×577.

$$\text{Weight matrix} = \begin{bmatrix} w_{1,1} & w_{1,2} & \cdots\cdots & w_{1,577} \\ w_{2,1} & w_{2,2} & \cdots\cdots & w_{2,577} \\ w_{3,1} & w_{3,2} & \cdots\cdots & w_{3,577} \end{bmatrix} \tag{3.4}$$

It is important to note that a bias is added with input. This bias allows the training model to shift the activation function to the right or left [52].

An effective strategy for initialization of weights suggested by Glorot et al [53] is to randomly select values for weight uniformly in the range [-β_{init} , β_{init}]. β_{init} can be calculated based on the equation 3.5 , where *f-in* is the

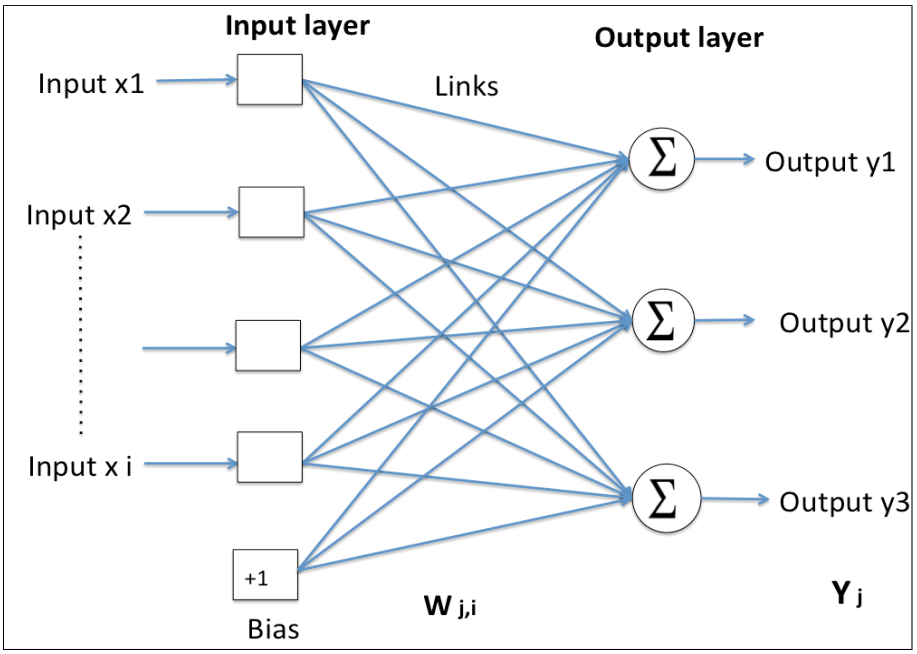

FIGURE 3.3: Basic structure of single layer Artificial Neural Network.

number of weights and *f-out* is the number of output nodes.

$$\beta_{init} = \frac{\sqrt{6}}{\sqrt{f\text{-}in + f\text{-}out}} \tag{3.5}$$

Input nodes are passive, they receive a single feature value and then feed it to the multiple output layers or hidden layers. Output layers multiply these input data with its corresponding weight and sum over all as described in equation 3.6. Feed forward propagation is depicted in figure 3.4.

$$z_j = \sum_{i=1}^{577} x_i w_{j,i} \tag{3.6}$$

The output of ANN is calculated by introducing equation 3.6 into the activation function. A common example of activation function is sigmoid function which is defined in formula 3.7. Sigmoid function is monotonically increasing function which is constrained by horizontal asymptotes as the input reaches $\pm\infty$ [54].

$$a_j = \frac{1}{1 + e^{-z_j}} \tag{3.7}$$

Sigmoid function limits the real valued input in to a range between 0 and 1. An example of sigmoid function is shown in figure 3.5.

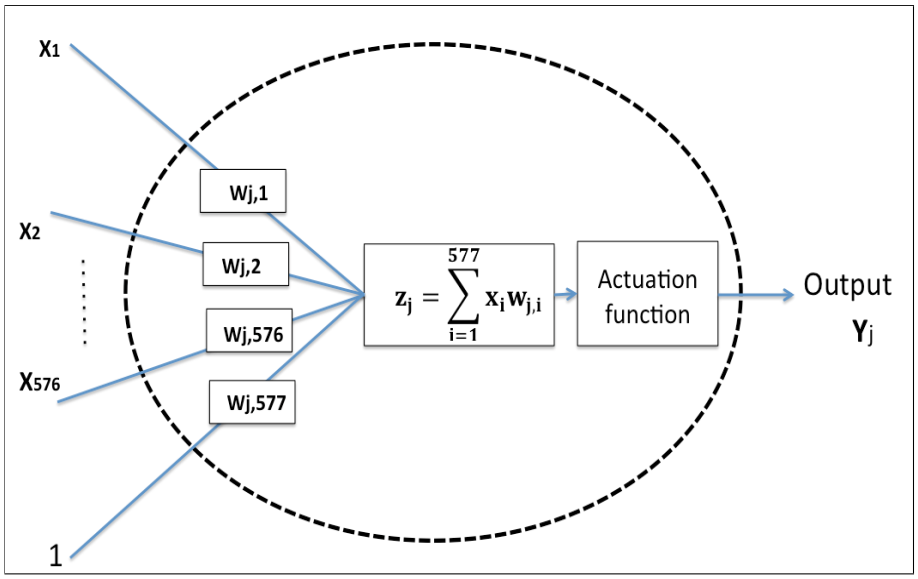

FIGURE 3.4: Illustration of Artificial Neural Network perceptron working.

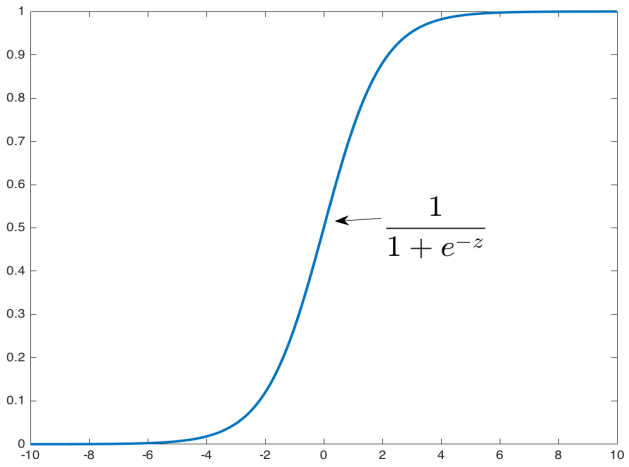

FIGURE 3.5: Sigmoid function.

Then the error for j^{th} output node is calculated from the difference between desired output of node j and current activation of node.

$$e_j = y_j - a_j \tag{3.8}$$

Perceptron learning is performed by *back propagation* method. In this method the error signal calculated for each output node is propagated backwards from output to input. The weights are updated with Δw_{ji} according to the formula 3.9.

$$w_{ji} = w_{ji} + \Delta w_{ji} \tag{3.9}$$

These Δw_{ji} were calculated from the error signal of the each output node.

$$\Delta w_{ji} = \alpha e_j x_i \tag{3.10}$$

α in equation 3.10 represents the learning rate. Since gradient of weight is multiplied with learning rate, it is crucial to select suitable learning rate. If learning rate is too small, the neural network result will be stuck in the local optimal and the learning process becomes too slow. If alpha is too large, the result will oscillate and fail to get a stable weight.

3.4 Features for neural network

The performance of a classifier is highly influenced by the selection of suitable feature vectors. A feature descriptor helps to simplifies the representation of an image patch into useful information by discarding the extraneous information. Feature vectors generated for the Artificial Neural Network are discussed in subsection 3.4.1 and 3.4.2.

3.4.1 Histogram of Oriented Gradients (HOG) features

HOG is an acronym for Histogram of Oriented Gradients. HOG can represent an image as it's local histogram [55]. Local object appearance and shape within an image can be explained with the distribution of intensity gradients in Histogram of Oriented Gradient descriptors. There are three steps to compute the HOG as demonstrated in figure 3.6. Prior to the implementation of these steps an image is divided in to cells of 4×4 pixels.

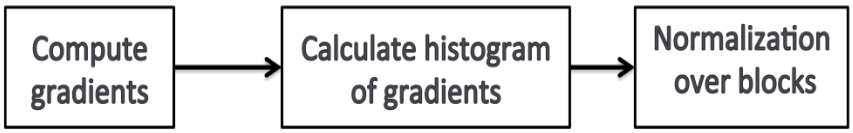

FIGURE 3.6: Steps for calculation of HOG features.

The first step for the computation of the HOG is to calculate the gradient of the image. The gradient computation is performed by filtering the image with horizontal and vertical derivative filter.

$$x = \begin{bmatrix} -1 & 0 & 1 \end{bmatrix} \quad \text{and} \quad y = \begin{bmatrix} -1 \\ 0 \\ 1 \end{bmatrix} \tag{3.11}$$

The magnitude and orientation of the gradient are computed as shown in formula 3.12.

$$G = \sqrt{G_x^2 + G_y^2} \quad \text{and} \quad \theta = tan^{-1}\left(\frac{G_y}{G_x}\right) \tag{3.12}$$

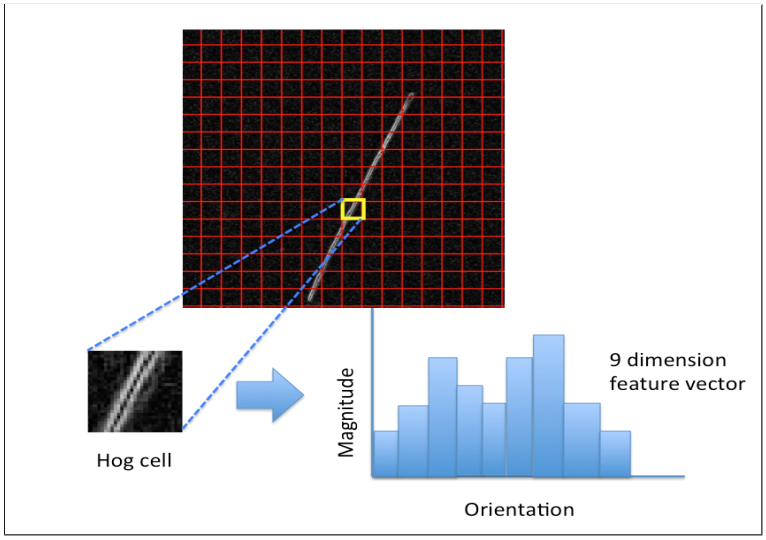

FIGURE 3.7: Gradient image is divided in to non-overlapping HOG cells. Each HOG cell consist of 4×4 pixels.

The second step in calculation of HOG is to find the histogram of gradients over each cell. Histogram is calculated for each pixel in each cell with x axis being orientation and y axis being gradient magnitude as shown in figure 3.7. The histogram channels spread evenly between $0°$ to $180°$ for unsigned bin (9 bin) and $0°$ to $360°$ (18 bin) for signed bin. Dalal et al [24] in their experiment found that 9 bin histogram gave better results than 18 bin histogram.

In the final step of computation of histogram, four cells are grouped together to form a 2×2 overlapping blocks as shown in figure 3.8. The feature vector of each cell in block is concatenated to form a 1×36 feature vector. Then feature vectors of all blocks are combined and normalized by its total magnitude. This reduces the effect of illumination and shadowing. A 20×20 image patch contains 16 overlapping blocks. The size of the feature vector for a 20×20 image patch with a cell size of 4×4 is 1×576. Smaller cell size increases the size of the feature vectors. Visualization of HOG features are illustrated in figure 3.9.

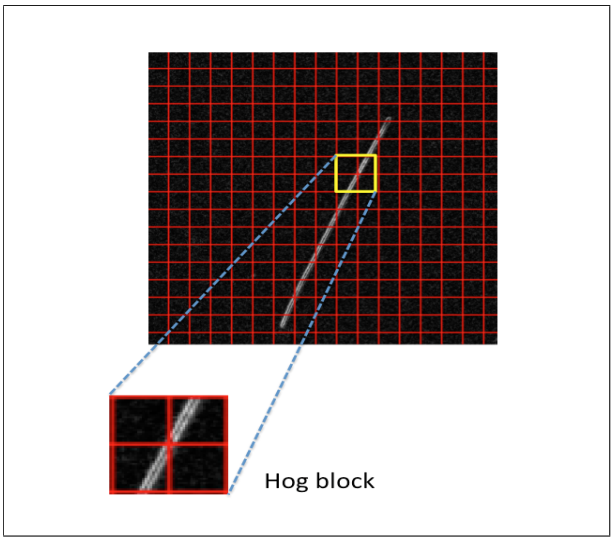

FIGURE 3.8: Representation of HOG block. A HOG block consists of 2×2 cells. 20×20 image contains 16 overlapping HOG blocks.

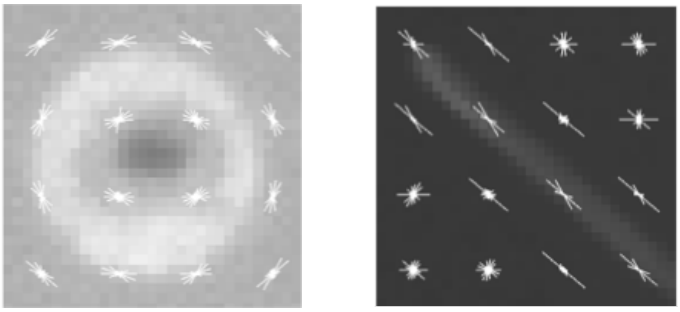

(A) HOG applied on dirt (B) HOG applied on scratch

FIGURE 3.9: Visualization of HOG feature on dirt and scratch

The HOG features are visualized with rose plots in MATLAB. The sixteen rose plots correspond to sixteen HOG blocks and each petal length corresponds to the gradient magnitude of each orientations. It is obvious from figure 3.9 that HOG feature can give a clear distinction between dirt and scratch image.

In the next subsection another feature set known as Hu moment tested for the generation of ANN model is discussed.

3.4.2 Hu moments

Hu moments are generated for each patch of the image for ANN model learning. Prior to the calculation of Hu moments, it is required to calculate raw moments and central moments. Raw image moment can be calculated as

follows:

$$M_{ij} = \sum_x \sum_y x^i y^j I(x, y), \tag{3.13}$$

where (x, y) is the image coordinate and I(x, y) is the corresponding intensity of the image.

$$\begin{aligned} M_{00} &= \sum_x \sum_y I(x, y) \\ M_{10} &= \sum_x \sum_y x I(x, y) \\ M_{01} &= \sum_x \sum_y y I(x, y) \end{aligned} \tag{3.14}$$

M_{00} is the zero order moment and M_{01} and M_{10} are the first order moments. M_{00} represents sum of grey level in an image. First order moments contain information about the center of gravity of the object $(\bar{x}, \bar{y})$.

$$\bar{x} = \frac{M_{10}}{M_{00}}, \quad \bar{y} = \frac{M_{01}}{M_{00}} \tag{3.15}$$

Raw image moments reduced by centroids lead to translational invariant central moment. It is calculated as follows:

$$\mu_{pq} = \sum_x \sum_y (x - \bar{x})^p (y - \bar{y})^q I(x, y) \tag{3.16}$$

Central moment is dependent on the size of the object in an image. For example, image of an object taken from different distance has different size. In 1962 Hu proposed HU moments [56] for visual pattern recognition. Hu momenta are rotational, scale, translational invariant. It is calculated from first, second and third order central moments. The equation 3.17 shows the calculation steps for Hu moments.

$$\begin{aligned} h_1 &= \mu_{20} + \mu_{02} \\ h_2 &= (\mu_{20} - \mu_{02})^2 + 4\mu_{11}^2 \\ h_3 &= (\mu_{30} - 3\mu_{12})^2 + (3\mu_{21} - \mu_{03})^2 \\ h_4 &= (\mu_{30} + \mu_{12})^2 + (\mu_{21} + \mu_{03})^2 \\ h_5 &= (\mu_{30} - 3\mu_{12})(\mu_{30} + \mu_{12})[(\mu_{30} + \mu_{12})^2 - 3(\mu_{21} + \mu_{03})^2] + (3\mu_{21} - \mu_{03}) \\ &\quad (\mu_{21} + \mu_{03})[3(\mu_{30} + \mu_{12})^2 - (\mu_{21} + \mu_{03})^2] \\ h_6 &= (\mu_{20} - \mu_{02})[(\mu_{30} + \mu_{12})^2 - (\mu_{21} + \mu_{03})^2] + 4\mu_{11}(\mu_{30} + \mu_{12})(\mu_{21} + \mu_{03}) \\ h_7 &= (3\mu_{21} - \mu_{03})(\mu_{30} + \mu_{12})[(\mu_{30} + \mu_{12})^2 - 3(\mu_{21} + \mu_{03})^2] - (\mu_{30} - 3\mu_{12}) \\ &\quad (\mu_{21} + \mu_{03})[3(\mu_{30} + \mu_{12})^2 - (\mu_{21} + \mu_{03})^2] \\ h_8 &= \mu_{11}[(\mu_{30} + \mu_{12})^2 - (\mu_{03} + \mu_{21})^2] - (\mu_{20} - \mu_{02})(\mu_{30} + \mu_{12})(\mu_{30} + \mu_{21}) \end{aligned} \tag{3.17}$$

3.4.3 Data set for neural network

Another important component of artificial neural network is training of the model using input *train data set*. The outputs that the model should produce corresponding to each data in the input data set is known. In case of any deviation from the desired output the weights of the model are adjusted so that the error at the output nodes are minimized. The trained ANN model is then validated using a data set called *validation data set*. In the validation stage the output of the model is compared to that of the actual output of the validation data set and the model with the best performance against the actual output is selected as final model. After validation the final model is tested for it's performance using a data set which is referred to as *test data set*. The performance level obtained at the test phase is the level of surety we can use while using the model for classification of a data set whose outcomes are not known.

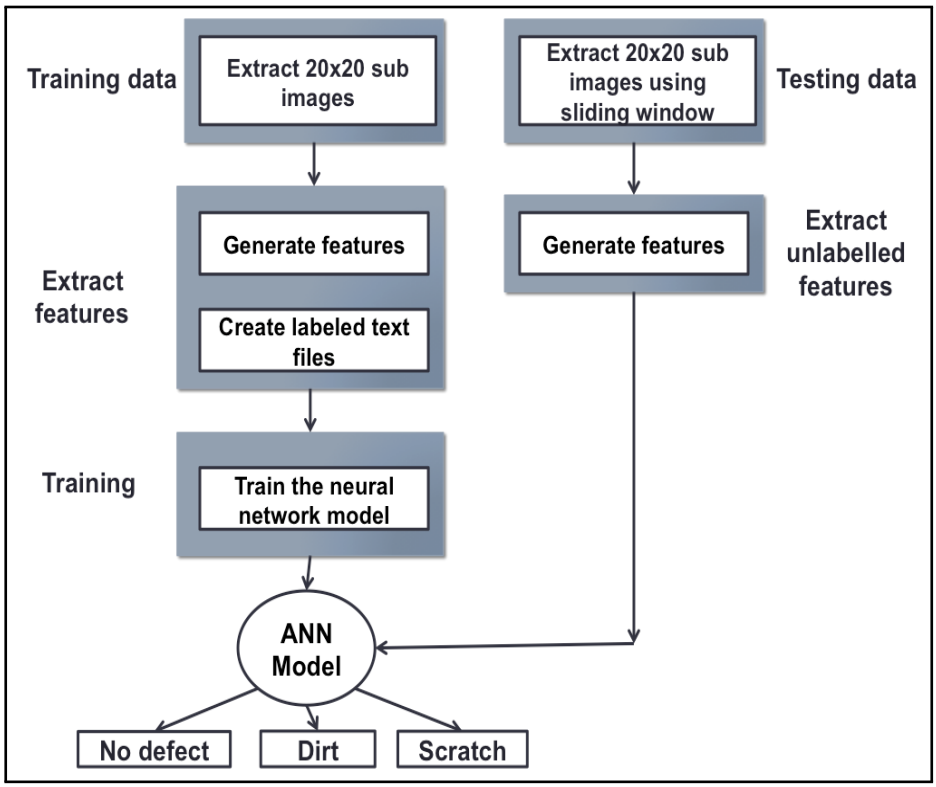

FIGURE 3.10: Block diagram representation of Artificial Neural Network training and testing phase.

The data set used in this work is collected from the test slabs gathered from painting work shop. The data set consist of 300 images with an image size of 2448 x 2048 pixels each in .bmp format. The image set includes scratches, dirt and no defect area. These images were captured with a monochrome camera under ring light illumination. Examples from each data set are shown in figure 3.11.

An approach to divide the data set for training and testing as suggested by Weimer et al. [21] is adopted in this work. 70 % of data set is used for training and 30% of data set is used for testing. The training data set consists of 500 image patches and testing data set consists of 150 image patches. Only images inside the circular reflection of ring light are extracted for training and testing.

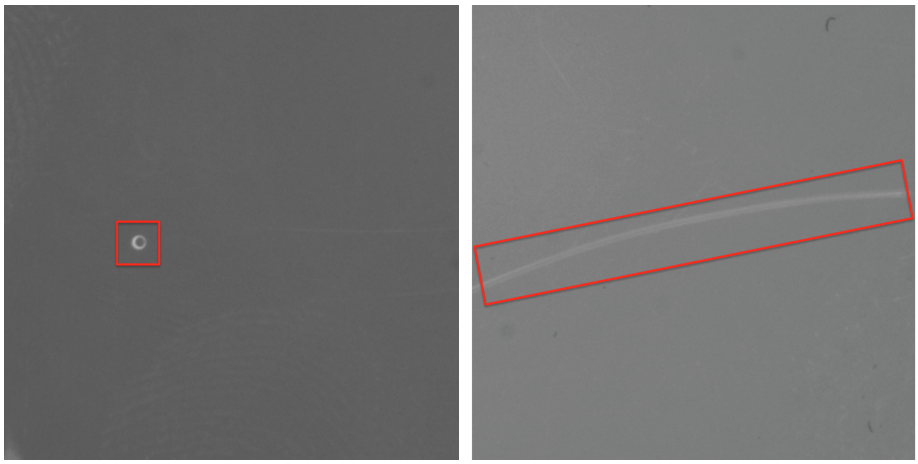

(A) Dirt image (B) Scratch image

FIGURE 3.11: Examples of data set used for ANN model generation.

The training data is created by extracting 20×20 image patches of positive and negative images. The size of the image patch is selected based on size of the defect. For a ring light setup in order to capture a defect of size 0.3 mm the optimal working distance of camera is set to 10 cm and focal length is adjusted to 16 mm. With this information the size of the defect on image can be calculated from magnification formula. The formula 3.18 represents the magnification of an object in an image [57].

$$m = \frac{D}{f} - 1, \tag{3.18}$$

where f represents the focal length and D represents working distance and m represents magnification. Calculations reveals that defect size of 0.3 mm has a size of 0.057 mm in an image. With a camera sensor having one pixel size equal to 3.45 μm this defect size is equivalent to 17 pixel in an image. The image patch should be atleast 20×20 in order to include a defect of size 0.3 mm.

Training data is labeled text files. The labels were 1 for no defects 2 for dirt and 3 for scratches. For the testing, images inside the circular reflection of ring light with a size 500×500 pixels were cropped. Image patches of size 20×20 pixels were extracted from this cropped images in sliding window fashion. Sliding window is performed in a way that, the image is divided into overlapping windows of size 20×20 pixels with an overlap of 10 pixel

in x and y direction. An example of sliding widow is demonstrated in figure 3.12. A 500×500 image contains 2401 image patches. The features extracted from these unlabeled patches and were then feed to the trained ANN model for the defect detection.

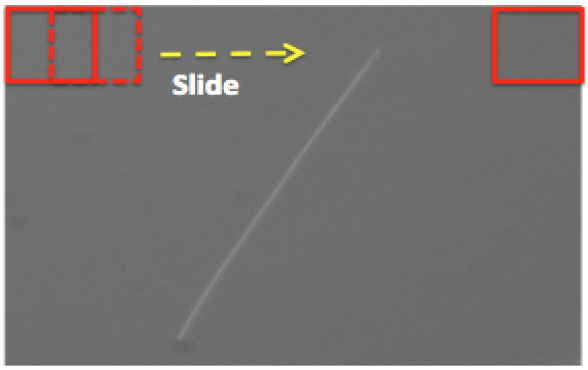

FIGURE 3.12: Illustration of sliding window function utilized in testing phase of ANN model.

3.4.4 Receiver Operating Curve (ROC)

Thamer et al [21] evaluated the performance of the ANN classifier using Receiver Operating Curve (ROC). Kevin et al [58] explained how to generate a ROC curve for two class artificial neural network. Since our problem is a multi-class problem (no defect, dirt, scratch), ROC for no defect class is plotted by considering no defect as one class and dirt and scratch together as defect class (no defect class vs defect class).

The x-axis of ROC is defined by false positive rate (FPR) and y-axis of ROC curve is defined by true positive rate (TPR).True positive rate is the percentage of defect samples that are correctly detected as defect samples. Or it can be defined as the ratio of true positives (TP) with respect to the total number of actual defect images P, TPR=TP/P. True positive is the number of correctly predicted defects. TPR is also known as sensitivity. The false positive rate (FPR) gives the ratio of false positives with respect to the total number of non-defect images N, FPR=FP/N. False positives (FP) are non-defect images miss-classified as defective images. False positive rate is also known as fall out.

ROC points are generated by varying the threshold value of output node activation. Threshold value is chosen in a range between 0 and 1. The node corresponding to the defect class is evaluated and if the value is greater than the threshold, image is classifiedd as positive. An ideal ROC has an area equal to one [21].

Chapter 4

Results

This chapter is structured as follows. Section 4.1 presents the results of various combinations of illuminations, camera and optics tested and final proposal for the machine vision system for fault detection on painted surface. Section 4.2 shows defect enhancement with various computer vision techniques. This includes results of morphological operations, Gabor filter, wavelet transform etc. The last section of this chapter presents classification of defect based on Artificial Neural Network classifier.

4.1 Image acquisition system

The key steps in selection of machine vision system include selection of camera which is able to capture target image and suitable optics for camera that can focus on to the surface of the target. The final step is the selection of appropriate illumination type that can increase the contrast between back ground and defect. Even though this aspect is vital, often it is not paid the attention it requires.

The final setup selection is based on the following criteria:

- Stability in performance irrespective of color,
- Stability in performance irrespective of color type category,
- Stability in performance irrespective of curved surface,
- Stability in performance irrespective of ambient light condition,
- High contrast between dirt and background surface,
- High contrast between crater and background surface.

Painted surface is available in different colors, hence the faults detection stability of machine vision system with various colors is a key factor. The base coat in painting determines final appearance as solid, metallic and pearl type color category. The sparkling effect of pearl and metallic surface with lighting cause speckles in the images of painted surface. This reduces the performance of various defect detection algorithms and sometimes these speckles

may be missidentied as defect. A machine vision system with less sensitiveness to color category reduces these problems.

Even though all the experiments were performed on flat surfaces, fault detection performance of machine vision system was tested on curved painted surfaces. This verification is due to the fact that real painted truck surfaces contain lots of surface details including curves and edge regions.

4.1.1 Selection of camera

The first step in selecting a machine vision camera is to find out the minimum resolution required for the application. To obtain a better quality image it is critical to choose an image sensor that can capture smallest feature according to the application. Using the following formula, minimum resolution can be found from the field of view and size of the smallest feature to inspect [59].

$$\text{Minimum resolution} = 2\left(\frac{\text{Field of view}}{\text{Smallest feature size}}\right) \tag{4.1}$$

The calculations reveal that a typical defect of size 0.3 mm and a field of view of 200 mm x 100 mm (size of test slab) would required a minimum sensor resolution of 1333 x 666 pixels. A Basler ace 2.3 MP camera (1920 x 1200) or Gene Nano M2450 5.1 MP (2448 x 2048) are appropriate for this requirements. Since field of view of camera and sensor resolution is directly proportional, to cover larger area higher resolution camera is required. Higher resolution images complicate further processing of images. Other options to cover a larger area are either move the object under inspection to the field of view of the camera or use more cameras with overlapping field of view.

4.1.2 Selection of optics

To ensure the high performance of a machine vision camera, the camera should be connected with an appropriate optics. The factors that affect the selection of optics with suitable focal length are working distance, field of view and sensor size. The following formula gives this relationship [60].

$$\begin{aligned} f &= \frac{\text{Magnification} \times \text{Working distance}}{1 + \text{Magnification}} \\ \text{where,} \quad \text{Magnification} &= \frac{\text{Sensor size of camera}}{FOV} \end{aligned} \tag{4.2}$$

Gene nano M2450 has a sensor format of 2/3 ″ which is equal to 8.8 mm sensor size in diagonal. According to the equation 4.2 an application of working distance 200 mm and field of view of 100 mm would required a lens of focal length 16.17 mm. Kowa lens is appropriate for this requirement.

Another lens tested was telecentric lens. Even though telecentric lens can provide same magnification for all objects and can eliminate perspective distortion, it is not suitable for this application. Because telecentic lens has a field of view of 6 cm, working distance of 10 cm, telecentric depth of 1 .1 cm. Image quality can ensure only in its telecentric depth. Beyond this telecentric depth images are distorted.

4.1.3 Selection of Illumination

The types of illuminations tested can be categorized as dark field illumination, bright field illumination and structured illumination. A test matrix generated for the evaluation of illumination is demonstrated in figure 4.1.

Set up	Dome light	Coaxial light	Ring light	Deflectometry
Stability to color	×	✓	✓	✓✓
Stability to surface category	××	×	✓	✓✓
Stability to curved surface	✓	××	××	✓
Stability to ambient light condition	✓	✓	×	✓
Contrast between dirt & background on image	×	✓	✓✓	✓✓
Contrast between crater & background on image	××	××	××	✓✓

✓✓ : Very good
✓ : Good
×× : Very bad
× : Bad

FIGURE 4.1: Test matrix for used for the selection of setup. This test matrix is mainly based on illuminations.

Bright field illumination

In images, generated with bright field illumination the defects are recognized as darker than the background. The bright field illumination tested during the experiment include diffused dome light and coaxial light. The images captured under dome light have very poor contrast between defect and background. In addition, a round shape reflection pattern corresponds to the hole

in the dome is observed on the captured image due to the specular property of the slab surface. Hence dome light is ineffective for this particular application.

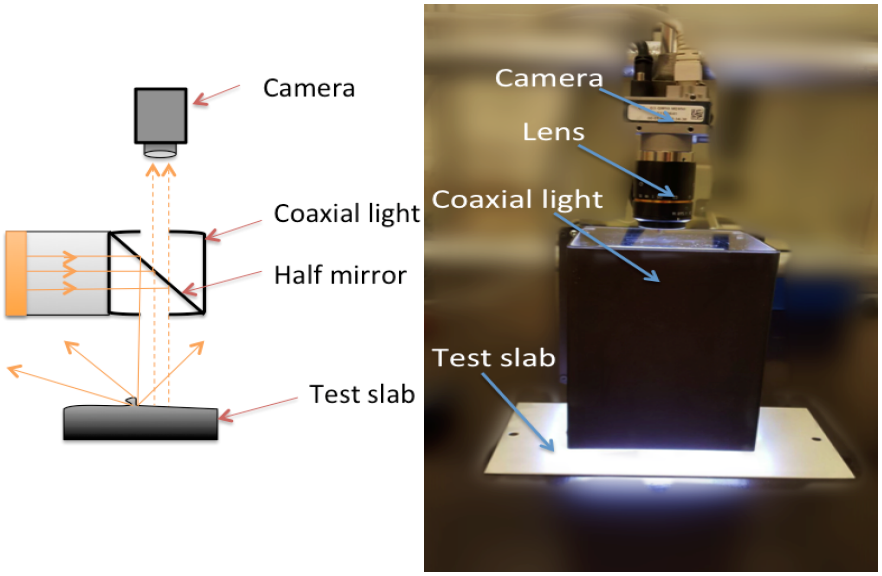

(A) Working principle of coaxial light setup (B) Photograph of coaxial light setup used

FIGURE 4.2: Coaxial light setup for defect detection on painted surface.

Figure 4.2 illustrates the working principle of coaxial light and photograph of experimental setup. A half mirror in coaxial light reflects light on to the target. The defect free region of target produces specular reflection and is allowed to pass through the half mirror to the camera. The light is diffusely reflected by the defects and this diffuse reflection is not allowed to pass through the half mirror. Image of a test slab captured with coaxial illumination is illustrated in figure 4.3.

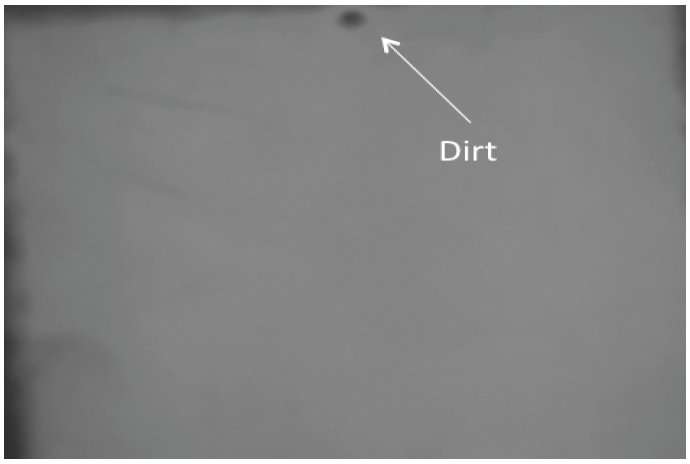

FIGURE 4.3: Image with dirt captured under coaxial illumination.

It can be observed that image is free of specular reflection. The image obtained from coaxial light illumination is acceptable but not good enough for further image processing. The defects are clearer near the shadow of coaxial light. Coaxial light required a close proximity to the object under inspection to make a contrast between defect and background which is not practical for a painted truck body inspection system.

Dark field illumination

Dark field illumination types that were tested includes IR ring light, RGB ring light and white ring light. The advantage of dark field illumination over bright field illumination is that the features of interest are highlighted with high contrast in image captured under dark field illumination. Thus comparatively less image processing effort is required for dark field illumination. Dark field illumination principle is shown in figure 4.4. The low angle light ray coming from ring light is reflected away from the specular target surface and light hits on defects will be reflected towards the camera.

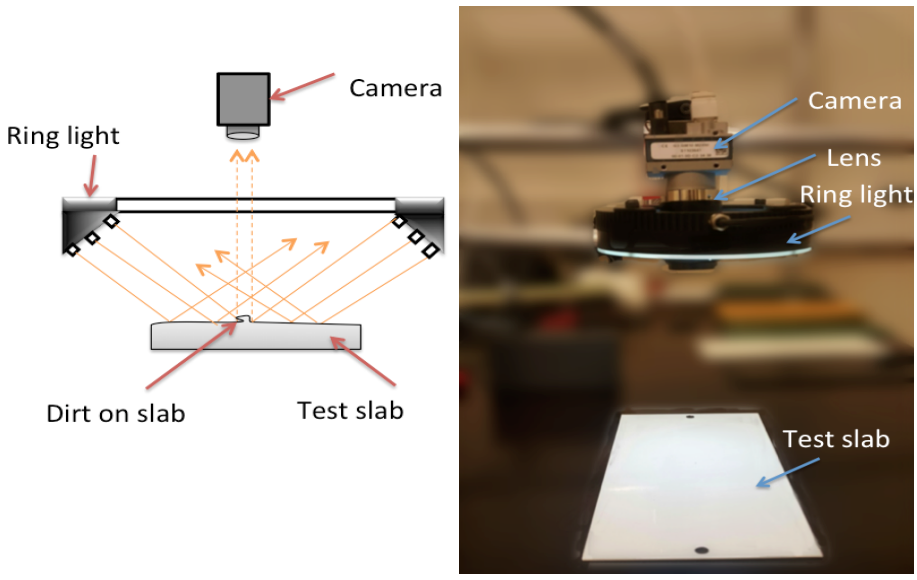

(A) Working principle of ring light setup (B) Photograph of ring light setup used

FIGURE 4.4: Ring light setup for defect detection on painted surface.

Hence the image captured mainly consists of dark regions in the absence of defects. The defects are captured as bright regions with dark background. Images captured with ring light is illustrated in figure 4.5. Since defects have high contrast inside the ring light reflection region, this image patch is extracted for further processing. This region is around 6 cm diameter. Hence in order to cover larger area, overlapping images should be append together.

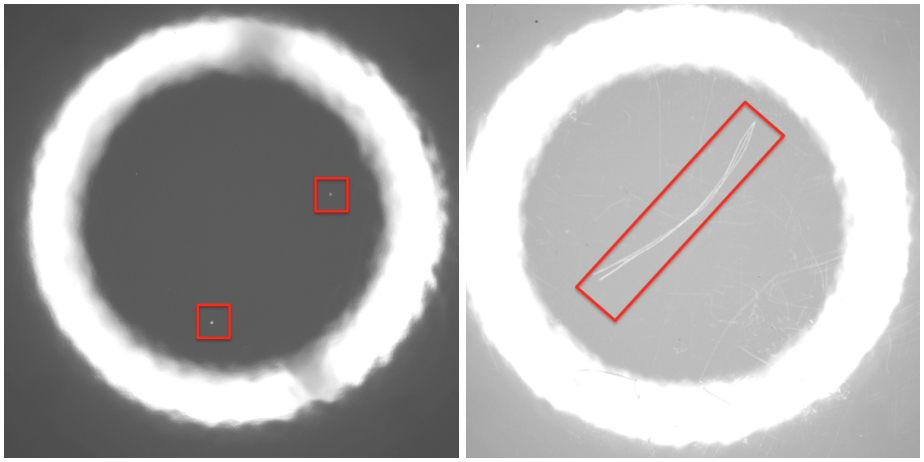

(A) Image with dirt (B) Image with scratch

FIGURE 4.5: Images captured under ring light illumination. Defects are marked inside the red boxes.

White ring light provide better images than RGB ring light for different color surfaces. Sometimes ambient light inside the experimental lab contributes brightness variations on the images which will affect quality of the image. IR ring light can eliminate this problem to a great extent.

Even though ring light setup can generate good enough images for solid surfaces, ring light could not avoid speckles in images of metallic painted surface. Computer vision methods like super pixel segmentation is employed to overcome this problem.

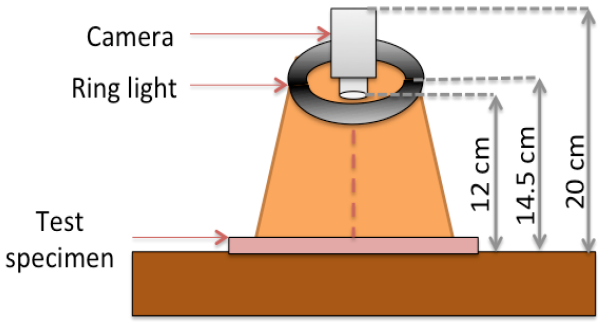

FIGURE 4.6: Schematic representation of ring light setup used.

A monochrome camera and a conventional lens is employed for the image acquisition. The optical axis of the camera is aligned normal to the surface of inspection. If the camera and ring light move farther away from the test object, the field of view of the camera will increase. But this causes a significant reduction in the visibility of minute defects in the captured images. An optimal position for camera, ring light and object under inspection obtained

after numerous trial and error experiments is illustrated in figure 4.6. The image is consistently free from the specular reflections if the lens tip is kept inside the ring illumination.

Structured illumination

Ring light setup is good enough for capturing defects like dirt. However, ring light setup was not effective for capturing crater (There is a crater inside the black circle which is not visible on image 4.7a). When the crater defect move towards a pattern like reflection of ring light, it can be visible on the image as illustrated in figure 4.7b. This reveals the potential of structured illumination for highlighting crater.

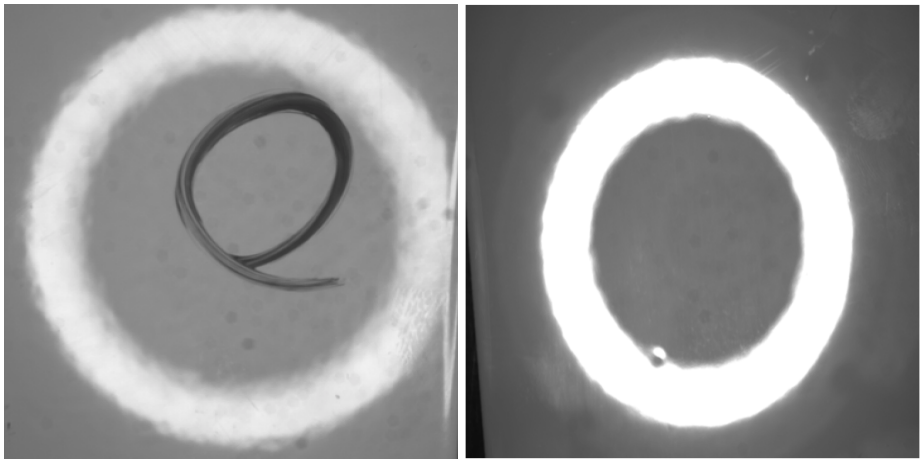

(A) Crater is not visible (B) Crater visible near ring pattern

FIGURE 4.7: Crater captured with ring light setup.

A sinusoidal pattern is projected on to the test slab with a LCD monitor as demonstrated in figure 4.8. The pattern is generated by MATLAB and has a frequency of 30 Hz and fringe width of 7 mm.

The light reflected on a specular surface obeys law of reflection. Hence the camera and screen should be placed with same angle. The camera captures the reflection of sinusoidal pattern from the test surface. The presence of defects causes distortion of the pattern. Another important thing to consider is that whether the camera should focus on the test surface or focus on the pattern. If the camera is focused on the pattern it would increase the resolution of pattern, but with blurred surface image. On the other hand camera focusing on the surface is able to capture image with high resolution for surface.

The lateral displacement of the pattern from its reference helps to calculate the slope of the pattern on test surface. This local slope helps to retrieve the height map of the surface. Since this work is mainly focused on intensity images, only simple computer vision algorithms are applied on the defelctometry images. The results are presented in the next section.

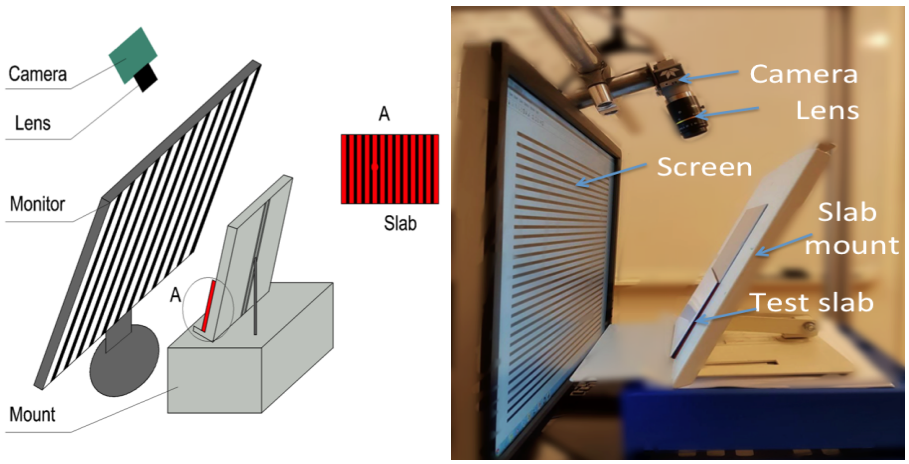

(A) Schematic of simple model of deflectometry setup

(B) Photograph of experimental deflectometry setup

FIGURE 4.8: Deflectometry setup for defect detection on painted surface.

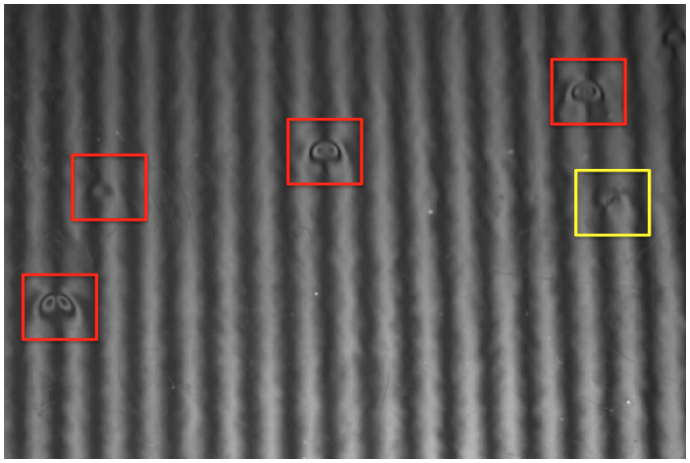

FIGURE 4.9: Image captured with deflectometry setup. Defects marked inside red boxes are craters and yellow box is dirt.

4.2 Computer vision methods for defect enhancement

In this work traditional image processing techniques like morphological operations, Gabor filters, wavelet transform etc were applied on the intensity and deflectometric images to highlight the defects. For metallic painted surfaces, super pixel segmentation was applied to do the same. All these results are presented in the following subsections.

4.2.1 Morphological operations

The images in figure 4.10 are used as the inputs for morphological operations, Gabor filter, wavelet transform method and super pixel segmentation.

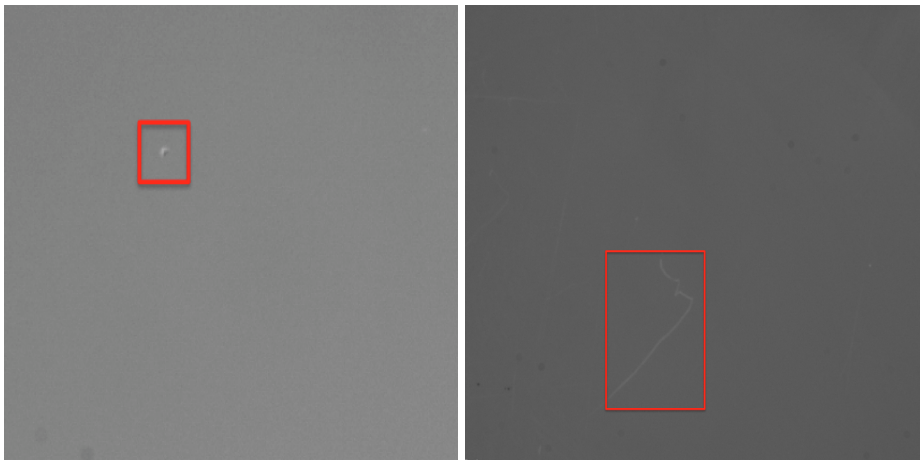

(A) Image with dirt (B) Image with scratch

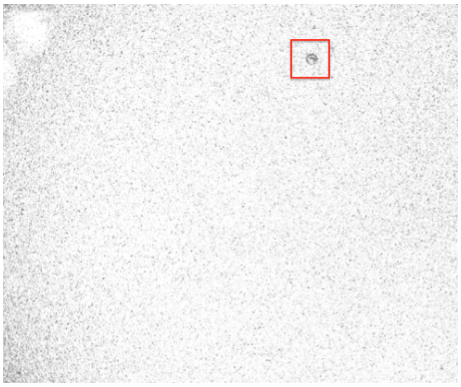

(C) Metallic surface with dirt

FIGURE 4.10: Images used for processing. The defects are marked inside the red boxes.

The basic morphological operations are erosion, dilation, opening, closing etc. When erosion is applied on the images, it removes pixels on the boundaries of the image. The value of the output pixel is the minimum value in the neighborhood of the input pixels. Size and shape of the structuring element determines the number of pixels removed. Therefore erosion operation results in shrinking of the defect in images captured with dark field illumination which have dark background and brighter defect region. So dilation is preferred over erosion.

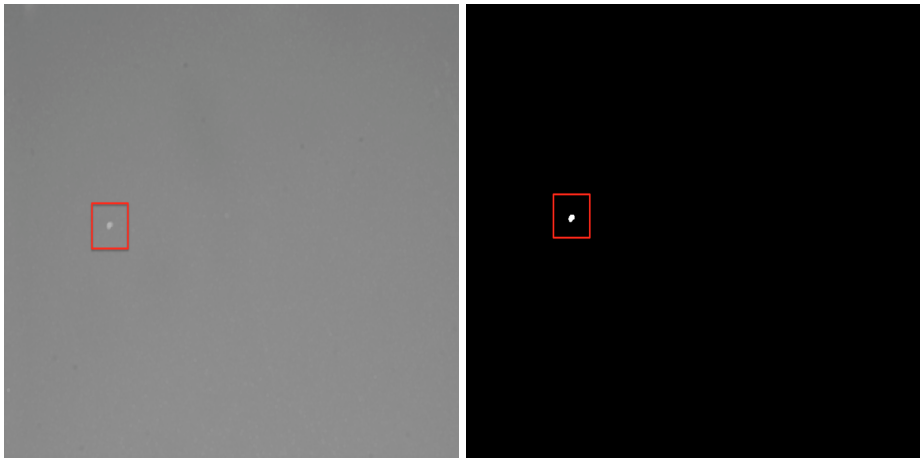

(A) Dilation on dirt image (B) After thresholding

FIGURE 4.11: Morphological operation on dirt image.

Dilation adds pixels to the boundaries of the image. The value of the output pixel is the maximum value in the neighborhood of the input pixels. So the defect is enlarged in images captured with dark field illumination.

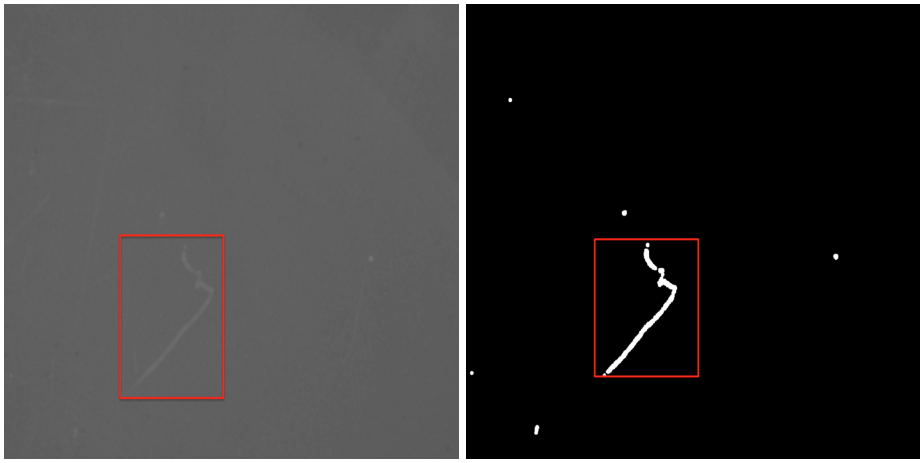

(A) Dilation on scratch image. (B) After thresholding

FIGURE 4.12: Morphological operation on scratch image.

When thresholding is applied to images after the morphological methods, the gray scale images are converted into binary images as shown in figures 4.11b and 4.12b. With the binary images, the defects could be differentiated from no defect areas with increased ease. One drawback with morphological methods is that the size of the defects in the image after the application of morphological methods is larger than the actual size of the defect.

4.2.2 Gabor filter

A Gabor filter bank was created in MATLAB where the inputs to the filter bank are orientation of the filter (in degrees) and wavelength (in pixels/cycle). The output of the filter bank is Gabor array. The real part of Gabor filter with different orientations (zero and ninety degrees) and wavelengths (ten and fifteen pixels/cycle) are shown in figure 4.13.

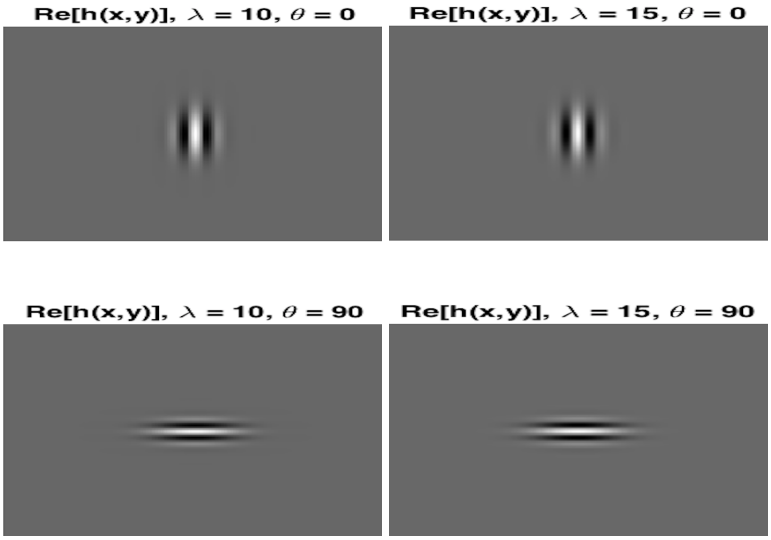

FIGURE 4.13: Real part of the filter in the Gabor filter array.

Gabor transform of dirt on solid surface is shown in figure 4.14. As evident from the figure orientation parameter of the filter bank does not play a huge role in highlighting the dirt.

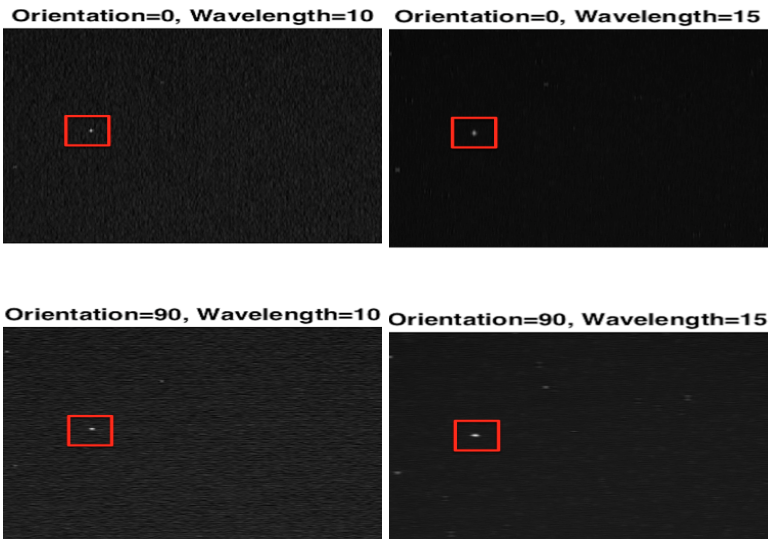

FIGURE 4.14: Gabor filtered image of dirt.

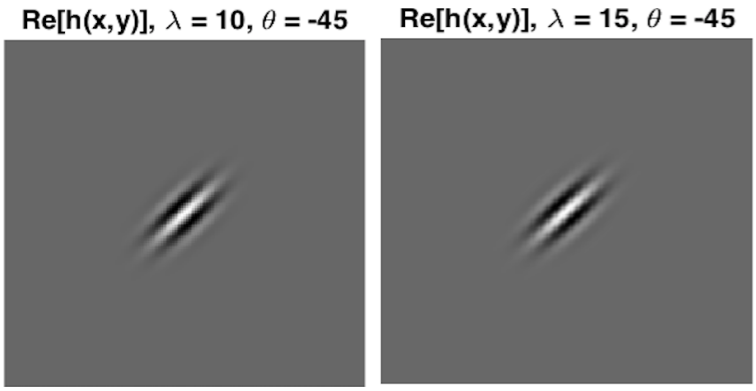

FIGURE 4.15: Real part of the Gabor filter array applied on scratch.

The orientation parameter of the Gabor filter bank should be chosen so that the alignment of the defects and Gabor filter are similar. This is evident from figure 4.16 where the scratch could be detected easily when the orientation is set as 45 degrees which is approximately equal to the orientation of the scratch. The orientation parameter is vital for the detection of scratch where as it is not so important for dirt.

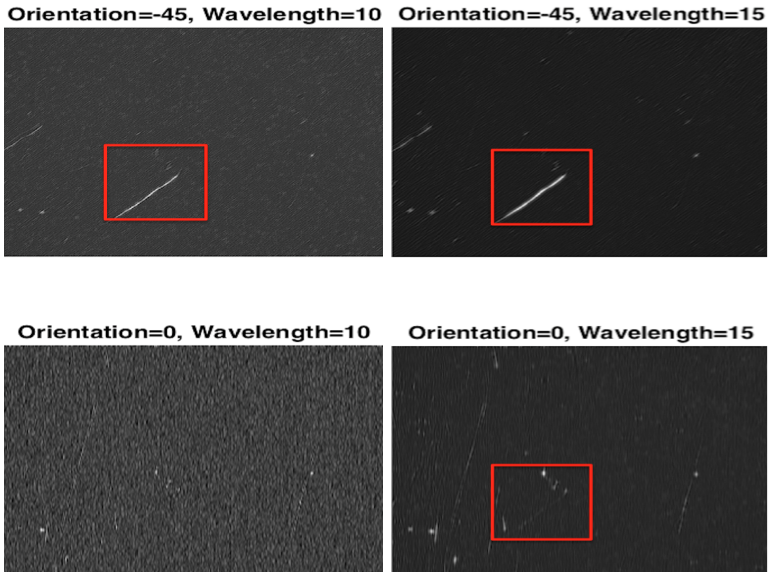

FIGURE 4.16: Gabor filtered image of scratch.

Gabor filter applied on deflectometry image is illustrated on figure 4.17. Here the deflectomtery image has vertical stripes. Hence Gabor filter with orientation equal to zero still retains the stripes which reduces the ease with which the defect could be detected. So an orientation of ninety degree reduces the stripes and enhance the visibility of defects. This in turn helps to avoid the stripes being mistaken for defects. This can be clearly observed from the figure 4.18. This images are obtained by applying thresholding on Gabor filtered images.

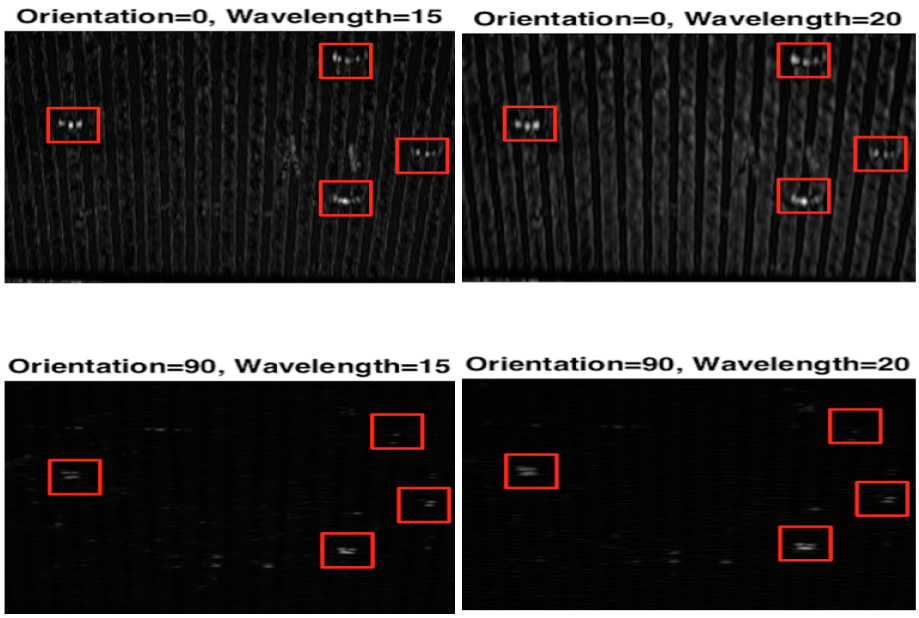

FIGURE 4.17: Gabor filtered deflectometric image.

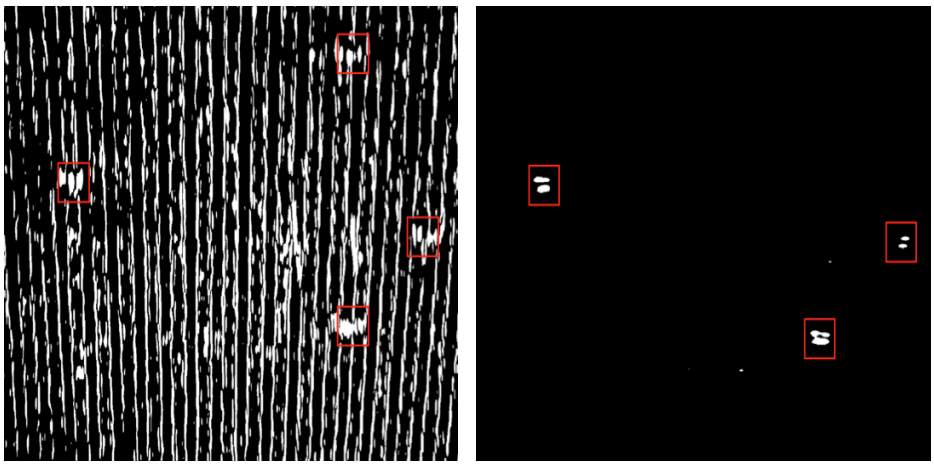

(A) Thresholding on Gabor filtered ($\theta = 0°$, λ=15) image

(B) Thresholding on Gabor filtered ($\theta = 90°$, λ=20) image

FIGURE 4.18: Thresholding performed on Gabor filtered image.

4.2.3 Wavelet transform

Even though there are several types of wavelet transforms, Haar wavelet transform method has been employed in this work. This method gave good results compared to methods like db1, db2 etc, during the trial and error phase.

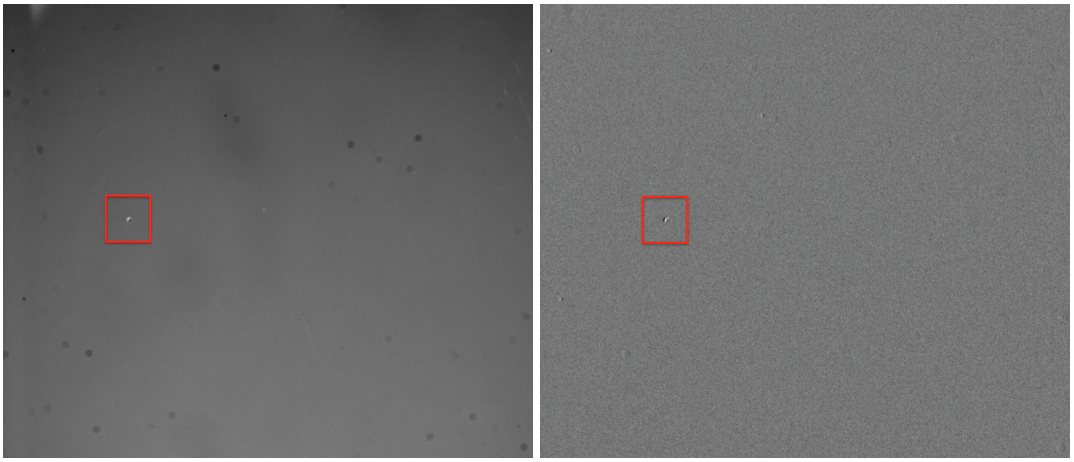

(A) Approximation Coefficient of Level 2 (B) Vertical detail coefficient of level 2

FIGURE 4.19: Haar wavelet transform of dirt.

Wavelet transform decomposes an image into approximation and detail components. Approximation components contain low frequency components of the image. Whereas detail components contains high frequency components of the image. There are vertical, horizontal and diagonal detail coefficients. Approximation coefficient gave an approximation of image. Since the edges of defects have high frequency, the defects are clearer on vertical detail coefficient which corresponds to high frequency rows. Haar wavelet transform of dirt and scratch on solid surface is illustrated in figure 4.19 and 4.20.

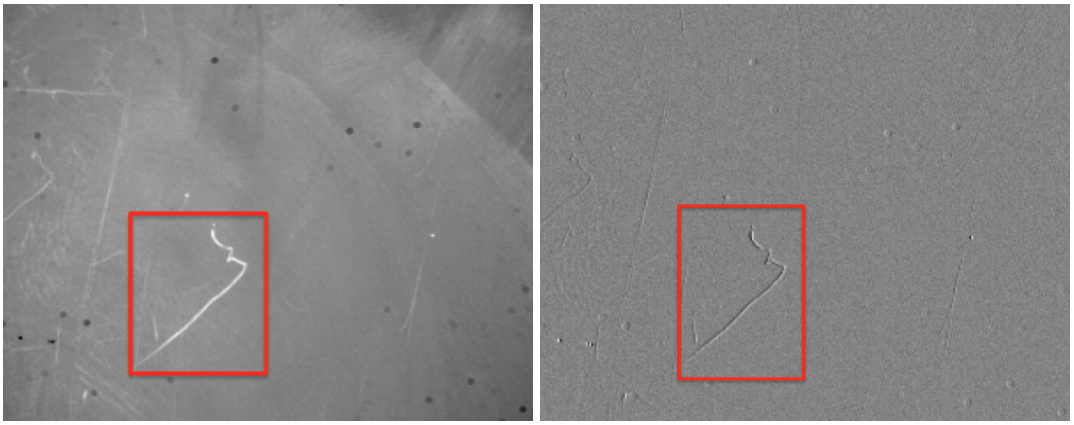

(A) Approximation Coefficient of Level 2 (B) Vertical detail coefficient of level 2

FIGURE 4.20: Haar wavelet transform of scratch.

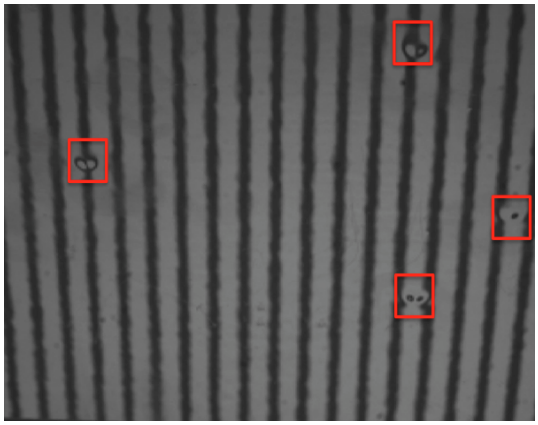

(A) Approximation Coefficient of Level 2

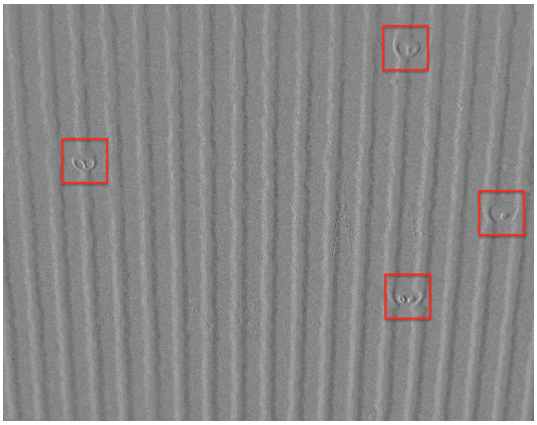

(B) Vertical detail coefficient of level 2

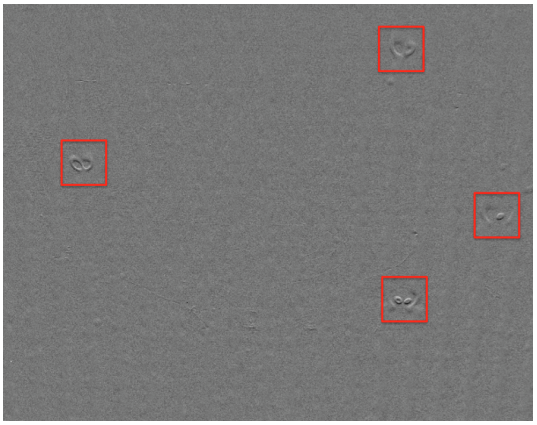

(C) Horizontal detail coefficient of level 2

FIGURE 4.21: Haar wavelet transform of deflectometry image.

As we can observe from the figures 4.19 and 4.20, the vertical coefficient highlights the defect region clearly whereas the approximation coefficient highlights even the minute details of the image which is not necessary for defect detection.

When horizontal detail component is applied on deflectometry image with vertical stripes, the vertical strips are avoided thereby highlighting just the defects. Similarly vertical detail component would be suitable to be applied on deflectometry image with horizontal stripes to obtain good results with defect detection.

4.2.4 Super pixel segmentation

For images of metallic surfaces methods like morphological operation, wavelet transform and Gabor filter are not suitable for defect enhancement. This is due to the fact that the images of metallic surface contain speckles which are also highlighted like defects while the above mentioned methods are used. This would increase the risk that the speckles be mistaken for defects. But super pixel segmentation method is superior to other methods in this respect.

(A) Dilation on metallic surface image (B) Thresholding after superpixel

FIGURE 4.22: Super pixel segmentation on metallic surface image.

Super pixel segmentation can divide an image into non-overlapping super pixels and it reduces the complexity of segmentation with single pixels. This method cluster pixels that are closer and having similar color. For a metallic surface atleast 4000 super pixels are required to extract the defects.

4.3 Defect classification based on Artificial Neural Network

Even though all the above discussed methods were able to enhance the defects from its background, a defect classification was not performed with these methods. Hence machine learning algorithm was implemented in MATLAB in order to classify the images into three classes viz. no defect, dirt and scratch. The algorithm implemented is a single layer Artificial Neural Network consisting iteration of back propagation and sigmoid activation function. HOG features and Hu moments were tested for the learning process of the ANN model. However, the model built based on Hu moments did not give good results in classifying the images. Model with Hu moments could only achieve a predictive accuracy of less than 50%. The performance of the ANN model with HOG features was analyzed in the training phase and the model classified 92.1% of the images correctly. So HOG features of the images were used as data set to train the Neural Network and to generate a model. HOG feature vector size for a 20x20 image patch has a size of 1x576. Hence the size of the weight matrix including the bias for an ANN with three output nodes is 3x577. The learning rate for back propagation was chosen randomly. The learning rate used to obtain the final model was 0.0369. The time taken for training this model was found to be 59.256 minutes.

The data set used for training the ANN model consisted of 500 images. Out of the 500 images, 270 images were of no defect type, 104 images were of scratch type and 126 images were of dirt type. During the test phase model classified 91.47 % of the images correctly. The data set for test phase consisted of 150 images. The performance of the machine learning algorithm is summarized below.

- Predictive accuracy

  Predictive accuracy describes how accurate the ANN model classifies the test images. The predictive accuracy of the learned system was found to be 91.47 % during testing phase.

- Complexity

  Complexity is an analysis parameter which describes how simple the trained model is. The trained model is a single layer ANN model and its weights are a matrix of size 3x577. So it can be said that the model is relatively simple.

- Efficiency

  Efficiency describes the time needed for training. The time taken for training this model with HOG feature set was found to be 59.256 minutes.

- Robustness

  Robustness describes how well the trained model could classify the images that are noisy. In order to check the robustness, the image of the metallic surface is tested with the sliding window function as shown in figure 4.28. It is clear from the figure 4.28 that the robustness is bad as the speckles are wrongly detected as dirt and scratch.

- Scalability

  Scalability is the parameter which describes the performance of the system depending on the size of the data. The ANN model was tested with 50, 100 and 150 feature set. The system took 0.56 s, 0.90 s and 1.24 s respectively for the testing process. As it is evident from the time data, the time required for testing increases with the size of the test data set.

- Interpretability

  Interpretability describes how easily the output and operation of the system are understandable to human. The system gives integer outputs 1, 2 or 3 based on the classification decision the model makes. The model gives an output of 1 if the image is classified as no defect, 2 if the image is classified as dirt and 3 if the image is classified as scratch. The sliding window function in conjunction with the model could identify the position of the defects in the image. The sliding window function marks the area in the image with dirt in blue color and the area with

scratch in red color as illustrated in figures 4.26 and 4.27. Overall the output of the system is quite easy to understand and interpret.

4.3.1 Confusion matrix

Confusion matrix was made to analyze the performance of the ANN model as shown in the table below. The values of TP, FP, TN and FN are tabulated in the confusion matrix.

		Prediction	
		Positive	Negative
Actual	Positive	$TP = 107$	$FN = 6$
	Negative	$FP = 0$	$TN = 39$

TABLE 4.1: Confusion matrix for the ANN model.

The confusion matrix was calculated for a classification algorithm which classifies images into two classes viz: no defect class and defect class. This confusion matrix shows excellent performance of the ANN model with no images without any defects are classified as defective. Mean while only six non defective images are classified as defective.

4.3.2 Receiver Operating Curve for ANN model

ROC plots are plotted to visualize the performance of the system in classification of the images. ROCs are plotted for no defect detection, dirt detection and scratch detection. The ROCs for the three different classes are shown in figure 4.23, 4.24 and 4.25.

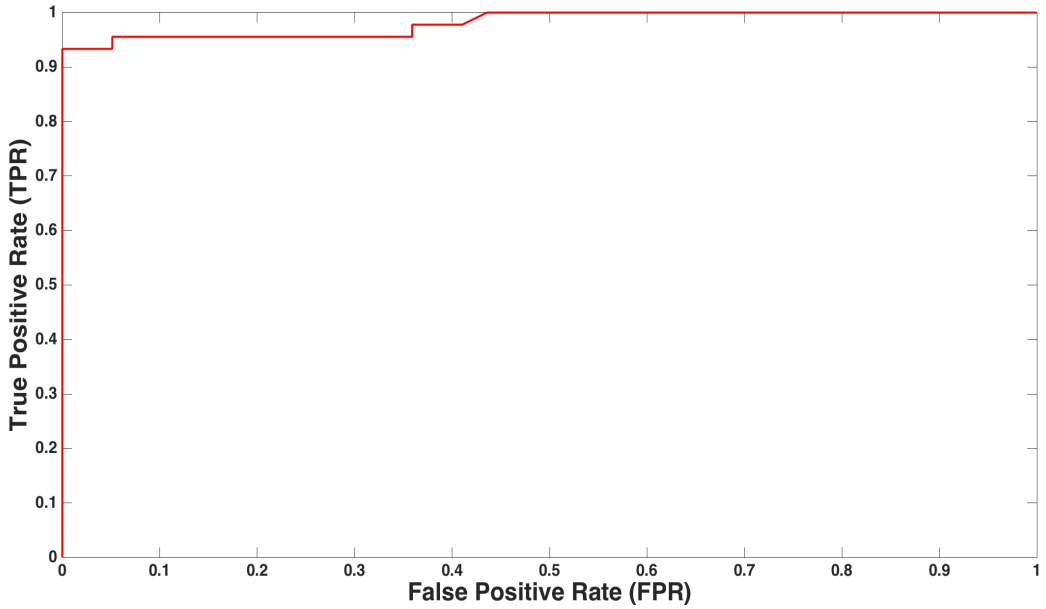

FIGURE 4.23: ROC plot for no defect class.

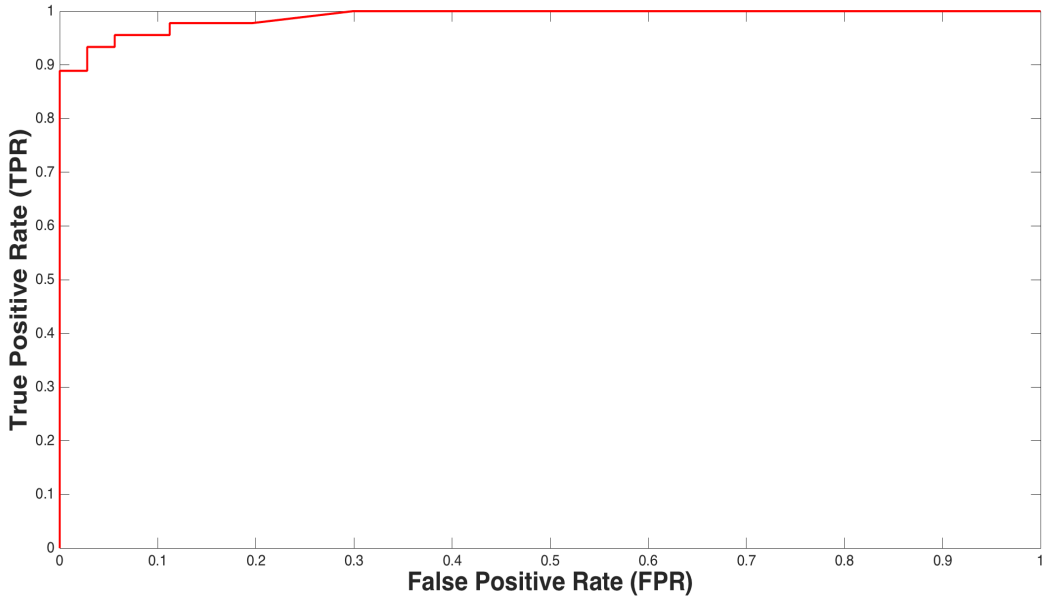

FIGURE 4.24: ROC plot for dirt class.

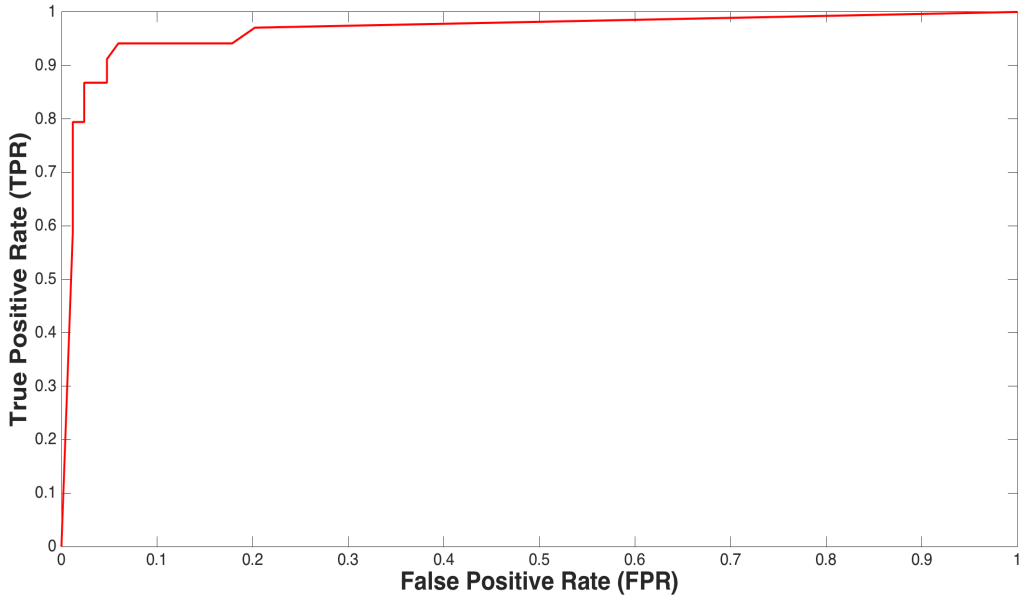

FIGURE 4.25: ROC plot for scratch class.

The defect detection system is doing a good job when it does not miss a defect. The system should detect a defect even if many non defect images are classified as defect images. This implies that the true positive rate should be close to one for the entire ROC plot. From the figure it is clear that ANN model is good, as the area under the curve is close to the maximum value for all the three classes.

4.3.3 Defect detection with Artificial Neural Network

The data set for training the ANN system consists of image patches which are of size 20x20. The image size was selected to be 20x20 in order to keep the size of the feature set at an optimal level so that the training of the system could be achieved in an acceptable time duration. This is advantageous for the ANN model to learn about small sized defects which otherwise may have a chance of being not detected in a big sized image. So in order to detect the defects in a bigger image (500x500) which is cropped inside the reflection of ring light, a sliding window function was implemented. Sliding window function scans through the entire image taking a part of the image with size of 20x20 at a time.Then the HOG feature set of the selected window is fed to the ANN model for classification. Windows classified as dirt is highlighted in blue color and the windows classified as scratch is highlighted in red color. The results obtained when the sliding window function is applied on images are shown in figure 4.26 and 4.27.

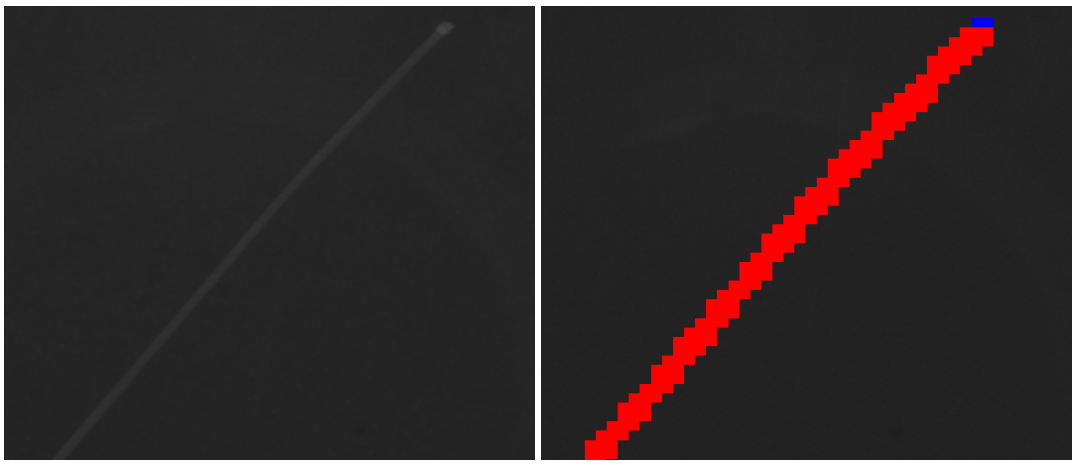

(A) Original scratch image (B) Detection result

FIGURE 4.26: Detection of scratch with ANN model. Blue color corresponds to dirt and red color corresponds to scratch.

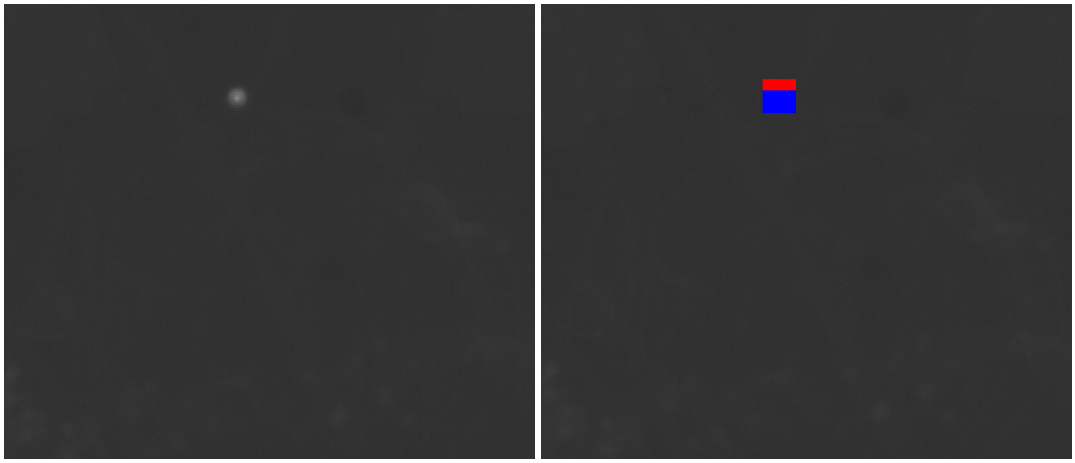

(A) Original dirt image (B) Detection result

FIGURE 4.27: Detection of dirt with ANN model. Blue color corresponds to dirt and red color corresponds to scratch.

From the figures 4.26 and 4.27 it can be observed that at the corners of the defects are classified incorrectly. This may be due to the fact that when the windows at the corners are taken for classification by sliding window function, the size of the defect might have not been good enough in the window for right classification.

In order to test the robustness of the ANN model, a metallic surface image was input to the sliding window function instead of the solid surface image. The result of the sliding window function on the metallic surface image is shown in figure 4.28.

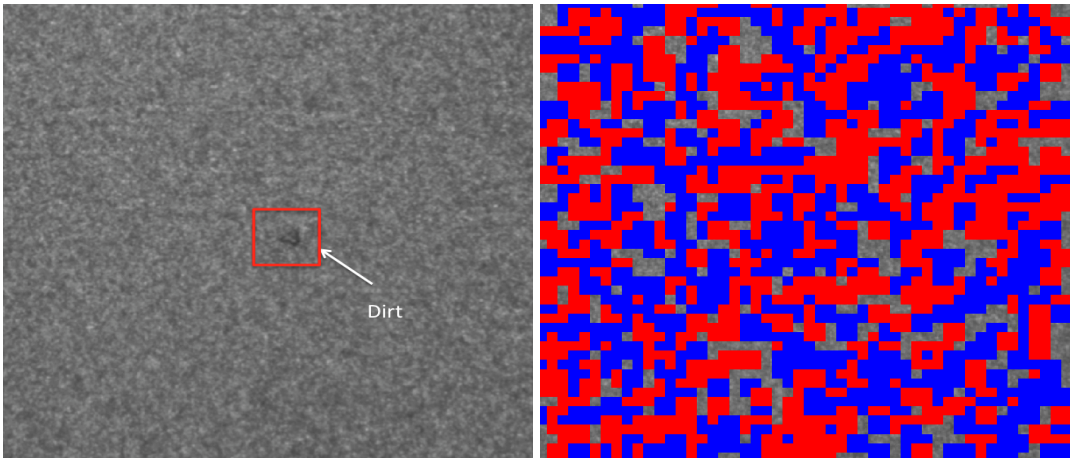

(A) Original dirt image (B) Detection result

FIGURE 4.28: Detection of dirt on metallic surface with ANN classification. Blue color corresponds to dirt and red color corresponds to scratch.

The figure 4.28 clearly shows that the robustness of the ANN model is very poor on metallic surface. Sparkles on the metallic surface is wrongly classified as dirt and scratches.

Chapter 5

Discussion and future work

Machine vision systems are increasingly used in quality control of painted surfaces. The main components of a machine vision system are camera, optics, illumination, image acquisition software and computer vision algorithms. It could be wrongly given too much importance to the camera part and completely neglect the illumination while designing a machine vision system. It was shown from this work that the illumination component is equally important component of the machine vision system especially for specular surface. This work also reveals that a good understanding about the nature of the surface being examined plays a vital role in the selection of machine vision system especially in the selection of illumination system. Three different kinds of illuminations were tested for specular surface namely bright field, dark field and structured illumination and out of these three, dark field and structured illumination (deflectometry) gave the best results. The deflectometry setup requires high level accuracy in terms of setting up and caliberations. The setup precision is not that important with dark field ring light setup compared to deflectometry setup. The proposed ring light setup could capture an area of 20x10 cm and in order to cover a much larger area either move the object under inspection to the field of view of the camera or use more cameras with an overlapping field of view.

The images of defects on the solid painted surface captured with ring light setup were enhanced using computer vision methods like morphological operations, wavelet transform, Gabor filter etc. For metallic surface due to the presence of speckles, super pixel segmentation was needed for highlighting the defects. However these methods were not able to classify the defect into classes which is essential for the repair unit and quality control unit. For classification of images based on defect type, a single layer Artificial Neural Network algorithm was employed. The possibility of using statistical features like Hu moments as a data set was not widely explored in this work because of the poor predictive accuracy of the ANN model trained with these feature vector as data set. One reason for the poor results with the Hu moments may be because of the fact that the values in the feature vector varied in large magnitude. In future, the feature vector could be tested as data set after normalizing the values of the feature vector. In this work HOG feature vectors of 20 x 20 image patches were extracted for the ANN model training. The

ANN model trained with HOG features of images as data set could give a clear distinction between dirt, scratch and no defect classes.

The quality of the images was found to be a very important factor influencing the correct classification of the images. Images with darker background and brighter defects gave excellent results with classification compared to brighter images. The higher the contrast between the background and the defects in the images, the better are the classification results. The image should only highlight the defects and rest of the surface should be darker and uniform in order to ensure high prediction accuracy. This indicates that image quality and illumination system are determining defect detection accuracy of a machine vision system for specular surface. However, the ANN model could not classify the images of metallic surfaces with speckles in a reliable manner as the speckles were misunderstood as dirt and scratch. The factors influencing the robustness of the algorithm should be investigated and they should be improved before employing the ANN model for classification of images that are noisy.

The size of the data set is an another factor affecting the performance of the machine learning algorithm. It was a time consuming process to capture lot of images and crop these images manually. Efficient and faster method to create a large data set could be something that should be developed.

The performance of the ANN model in classification of the images should be compared with that of other models based classifier algorithms like SVM classifier in future. This would help in establishing which algorithm gives better results with detection and classification of defects.

Appendix A

More figures of defect detection with ANN model

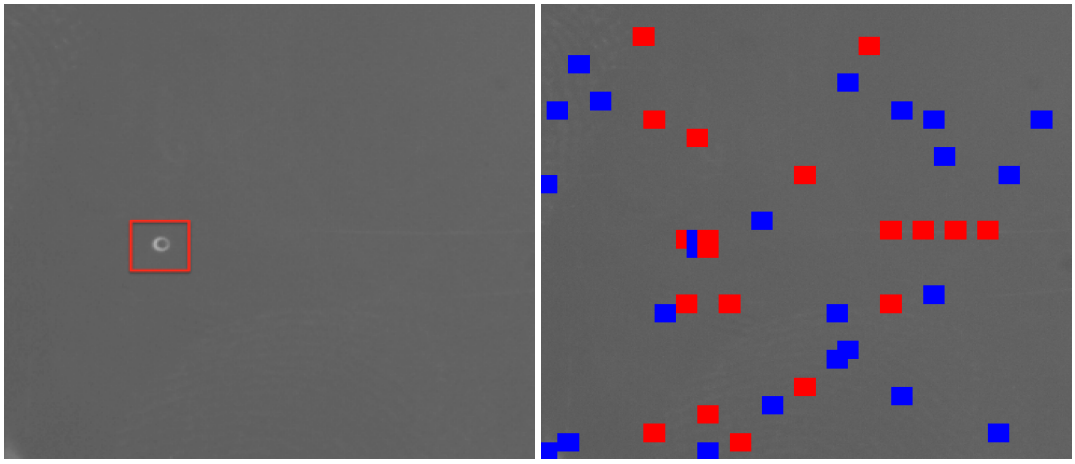

(A) Original dirt image (B) Detection result

FIGURE A.1: Detection of dirt with ANN model. Blue color corresponds to dirt and red color corresponds to scratch.

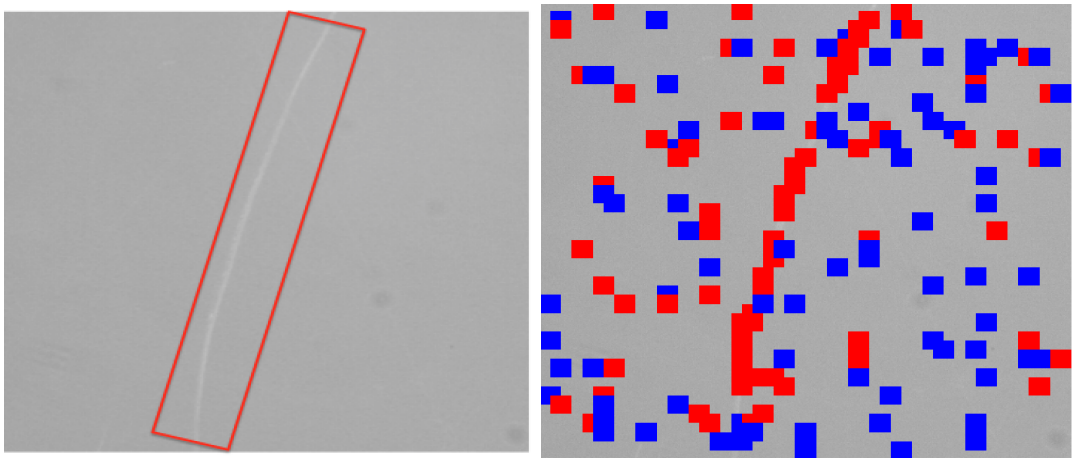

(A) Original scratch image (B) Detection result

FIGURE A.2: Detection of scratch with ANN model. Blue color corresponds to dirt and red color corresponds to scratch.

During defect detection with ANN model, some parts of no defect region is miss-classified as defect regions. This is due to the fact that images in A.1 and A.2 have brighter background and contrast between defect and background is not that good. The background has poor quality due to non uniform illumination. This indicates the importance of image quality to ensure good detection result with ANN model.

Bibliography

[1] Shiqing Ren and Yan Wang. "Separating reflection components of smooth metallic surface using special random sampling method". In: *3rd International Conference of Innovative Computing Information and Control* (2008), pp. 527–527.

[2] Michael Oren and Shree K Nayar. "Generalization of Lambert's reflectance model". In: *Proceedings of the 21st annual conference on Computer graphics and interactive techniques* (1994), pp. 239–246.

[3] Pradeep Gnanaprakasam et al. "Efficient 3D characterization of raised topological defects in smooth specular coatings". In: *Image and Vision Computing* 27.4 (2009), pp. 319–330.

[4] Chang Jiang Li et al. "Developing a new automatic vision defect inspection system for curved surfaces with highly specular reflection". In: *International Journal of Innovative Computing, Information and Control* 8.7B (2012), pp. 5121–5136.

[5] Nelson K Akafuah et al. "Evolution of the automotive body coating process—a review". In: *Coatings* 6.2 (2016), p. 24.

[6] Franz Pernkopf and Paul O'Leary. "Image acquisition techniques for automatic visual inspection of metallic surfaces". In: *NDT & E International* 36.8 (2003), pp. 609–617.

[7] F Puente Leon and S Kammel. "Inspection of specular and painted surfaces with centralized fusion techniques". In: *Measurement* 39.6 (2006), pp. 536–546.

[8] Ajay Kumar. "Computer-vision-based fabric defect detection: A survey". In: *IEEE transactions on industrial electronics* 55.1 (2008), pp. 348–363.

[9] Yud-Ren Chen, Kuanglin Chao, and Moon S Kim. "Machine vision technology for agricultural applications". In: *Computers and electronics in Agriculture* 36.2 (2002), pp. 173–191.

[10] Dave Litwiller. "Ccd vs. cmos". In: *Photonics Spectra* 35.1 (2001), pp. 154–158.

[11] Ronald A Petrozzo and Stuart W Singer. "Telecentric lenses simplify noncontract metrology". In: *Test & Measurement World* 21.13 (2001), pp. 4–4.

[12] Zhang Xue-Wu et al. "A vision inspection system for the surface defects of strongly reflected metal based on multi-class SVM". In: *Expert Systems with Applications* 38.5 (2011), pp. 5930–5939.

[13] Daryl Martin. "A practical guide to machine vision lighting". In: *Midwest Sales and Support Manager, Adv Illum2007* (2007), pp. 1–3.

[14] Ahmed Abouelela et al. "Automated vision system for localizing structural defects in textile fabrics". In: *Pattern recognition letters* 26.10 (2005), pp. 1435–1443.

[15] Timo Piironen et al. "Automated visual inspection of rolled metal surfaces". In: *Machine Vision and Applications* 3.4 (1990), pp. 247–254.

[16] Riby Abraham Boby et al. "Identification of defects on highly reflective ring components and analysis using machine vision". In: *The International Journal of Advanced Manufacturing Technology* 52.1-4 (2011), pp. 217–233.

[17] Markus C Knauer, Jurgen Kaminski, and Gerd Hausler. "Phase measuring deflectometry: a new approach to measure specular free- form surfaces". In: *Proceedings of SPIE* 5457.0 (2004), pp. 366–376.

[18] Sören Kammel and Fernando Puente León. "Deflectometric measurement of specular surfaces". In: *IEEE transactions on instrumentation and measurement* 57.4 (2008), pp. 763–769.

[19] Denis Perard and Juergen Beyerer. "Three-dimensional measurement of specular free-form surfaces with a structured-lighting reflection technique". In: *Intelligent Systems & Advanced Manufacturing* (1997), pp. 74–80.

[20] Xianghua Xie. "A review of recent advances in surface defect detection using texture analysis techniques". In: *ELCVIA Electronic Letters on Computer Vision and Image Analysis* 7.3 (2008).

[21] D Weimer, H Thamer, and B Scholz-Reiter. "Learning defect classifiers for textured surfaces using neural networks and statistical feature representations". In: *Procedia CIRP* 7 (2013), pp. 347–352.

[22] Zhihu Huang and Jinsong Leng. "Analysis of Hu's moment invariants on image scaling and rotation". In: *Computer Engineering and Technology (ICCET), 2010 2nd International Conference on* 7 (2010), pp. V7–476.

[23] F Tajeripour and E Kabir. "Defect detection in patterned fabrics using modified local binary patterns". In: *Conference on Computational Intelligence and Multimedia Applications, 2007. International Conference on* 2 (2007), pp. 261–267.

[24] Navneet Dalal and Bill Triggs. "Histograms of oriented gradients for human detection". In: *Computer Vision and Pattern Recognition, 2005. CVPR 2005. IEEE Computer Society Conference on* 1 (2005), pp. 886–893.

[25] Mohammad H Karimi and Davud Asemani. "Surface defect detection in tiling Industries using digital image processing methods: Analysis and evaluation". In: *ISA transactions* 53.3 (2014), pp. 834–844.

[26] Kai-Ling Mak, P Peng, and KFC Yiu. "Fabric defect detection using morphological filters". In: *Image and Vision Computing* 27.10 (2009), pp. 1585–1592.

[27] H Elbehiery, A Hefnawy, and M Elewa. "Surface Defects Detection for Ceramic Tiles Using Image Processing and Morphological Techniques." In: *WEC (5)* (2005), pp. 158–162.

[28] Anil K Jain and Farshid Farrokhnia. "Unsupervised texture segmentation using Gabor filters". In: *Pattern recognition* 24.12 (1991), pp. 1167–1186.

[29] Kamlesh Kumar et al. "Image edge detection scheme using wavelet transform". In: *11th International Computer Conference on Wavelet Active Media Technology and Information Processing* (2014), pp. 261–265.

[30] Shiqing Ren et al. "Inspection of Smooth Metallic Surface Using Complex Discrete Wavelet Transform". In: *3rd International Conference on Innovative Computing Information and Control* (2008), pp. 63–63.

[31] Kamil Zidek et al. "Embedded vision equipment of industrial robot for inline detection of product errors by clustering–classification algorithms". In: *International Journal of Advanced Robotic Systems* 13(5) (2016), p. 1729881416664901.

[32] AG Ramakrishnan, S Kumar Raja, and HV Raghu Ram. "Neural network-based segmentation of textures using Gabor features". In: *12th IEEE Workshop on Neural Networks for Signal Processing* (2002), pp. 365–374.

[33] Ajay Kumar. "Neural network based detection of local textile defects". In: *Pattern Recognition* 36(7) (2003), pp. 1645–1659.

[34] Stefan Karbacher et al. "Visualization and detection of small defects on car-bodies". In: *Modeling and Visualization , Sankt Augustin* (1999), pp. 1–8.

[35] Rodger L Reynolds et al. "Theory and applications of a surface inspection technique using double-pass retroreflection". In: *Optical Engineering* 32.9 (1993), pp. 2122–2129.

[36] H. Loferer. "Automatic Painted Surface Inspection and Defect Detection". In: *Proceedings SENSOR 2011* (2001), pp. 871–873.

[37] *Genie Nano C4030 Color - Product Detail - Teledyne DALSA*. http://www.teledynedalsa.com/imaging/products/cameras/area-scan/genie-nano/G3-GM10-M2450/. Accessed: 2017-08-03.

[38] *Basler Microscopy ace 2.3 MP, 1/1.2 in. format, C-Mount, 1920 x 1200*. https://graftek.biz/products/basler-microscopy-ace-2-dot-3-mp-1-slash-1-dot-2-in-format-c-mount-1920-x-1200-82-fps-color. Accessed: 2017-08-03.

[39] *TC23036 - Opto Engineering*. https://www.stemmer-imaging.se/media/uploads/optics/opto-engineering/en/en-Opto-Engineering-TC-23036-Bi-Telecentric-Lens-OOPEN23-201503.pdf. Accessed: 2017-08-03.

[40] *Kowa LM16JC10M 2/3" 16mm F1.8 Manual Iris C-Mount Lens, 10-Megapixel Rated*. http://www.rmaelectronics.com/kowa-lm16jc10m-2-3-16mm-f1-8-manual-iris-c-mount-lens-10-megapixel-rated/. Accessed: 2017-08-03.

[41] *Diffused Dome Light - Metaphase Technologies*. https://www.metaphase-tech.com/diffused_dome_tube_lights/diffused_dome_light. Accessed: 2017-08-03.

[42] *White led On-Axis 100x100*. http://www.phloxgc.com/datasheet/PHLOX_LEDW_OA_100x100_SLLUB_Q_1R_24V.pdf. Accessed: 2017-08-04.

[43] *LDR2-90IR2-85 CCS INC*. http://www.ccs-grp.com/products/model/3216. Accessed: 2017-08-04.

[44] *LDL2-266X30SW CCS INC*. http://www.ccs-grp.com/products/model/1491. Accessed: 2017-08-04.

[45] *Smart Color Box Test Light Multicolor Tester from Smart Vision Lights ...* https://smartvisionlights.com/products/accessories. Accessed: 2017-08-04.

[46] V Shiv Naga Prasad and Justin Domke. "Gabor filter visualization". In: *J. Atmos. Sci* 13 (2005), p. 2005.

[47] John G Daugman. "Uncertainty relation for resolution in space, spatial frequency, and orientation optimized by two-dimensional visual cortical filters". In: *JOSA A* 2.7 (1985), pp. 1160–1169.

[48] Marc Antonini et al. "Image coding using wavelet transform". In: *IEEE Transactions on image processing* 1.2 (1992), pp. 205–220.

[49] Radhakrishna Achanta et al. "Slic superpixels". In: *EPFL Technical Report 149300* (2010).

[50] Radhakrishna Achanta et al. "SLIC superpixels compared to state-of-the-art superpixel methods". In: *IEEE transactions on pattern analysis and machine intelligence* 34.11 (2012), pp. 2274–2282.

[51] Sun-Chong Wang. "Interdisciplinary computing in Java programming". In: *Springer Science & Business Media* 743 (2012).

[52] *Role of Bias in Neural Networks*. https://stackoverflow.com/questions/2480650/role-of-bias-in-neuralnetworks. Accessed: 2017-07-22.

[53] Xavier Glorot and Yoshua Bengio. "Understanding the difficulty of training deep feedforward neural networks". In: *Proceedings of the Thirteenth International Conference on Artificial Intelligence and Statistics* (2010), pp. 249–256.

[54] Genevieve B Orr and Klaus-Robert Müller. "Neural networks: tricks of the trade". In: *Springer* (2003).

[55] Frédéric Suard et al. "Pedestrian detection using infrared images and histograms of oriented gradients". In: *Intelligent Vehicles Symposium* (2006), pp. 206–212.

[56] Ming-Kuei Hu. "Visual pattern recognition by moment invariants". In: *IRE transactions on information theory* 8.2 (1962), pp. 179–187.

[57] *Optic basics - calculation of the optics*. http://www.vision-doctor.com/en/optical-basics.html. Accessed: 2017-07-25.

[58] Kevin Woods and Kevin W Bowyer. "Generating ROC curves for artificial neural networks". In: *IEEE Transactions on medical imaging* 16.3 (1997), pp. 329–337.

[59] *Calculating Camera Sensor Resolution and Lens Focal Length*. http://digital.ni.com/public.nsf/allkb/1BD65CB07933DE0186258087006FEBEA. Accessed: 2017-08-09.

[60] *Basics of Lens selection for machine vision cameras*. http://info.adimec.com/blogposts/bid/73803/Basics-of-Lens-Selection-for-Machine-Vision-Cameras. Accessed: 2017-08-09.